ADSORPTION OF POLY(VINYL ALCOHOL) ONTO POLYDIMETHYLSILOXANE SUBSTRATES: FORMATION OF CONTINUOUS FILMS, HONEYCOMB STRUCTURES, AND FRACTAL MORPHOLOGIES

AKCHHETA KARKI

Thesis advisor: Wei Chen

A thesis presented to the faculty of Mount Holyoke College in partial fulfillment of the requirements for the degree of Bachelor of Arts with honors

May 2015

Chemistry Department

We would like to thank the National Science Foundation for financial support.

ACKNOWLEDGEMENTS

I cannot express enough gratitude to Professor Wei Chen, without whom the writing of this thesis would not have been possible. From teaching my very first general chemistry class in college to guiding me through the writing of this thesis, Professor Wei's mentoring through every step of my undergraduate career has been remarkable. Thank you for inspiring me to constantly seek self-improvement and instilling in me a passion for research work that I never thought I had. This is perhaps the only section of my entire thesis that I have written without her help.

I am deeply grateful to Professor Darren Hamilton for his invaluable enthusiasm and support. I will be forever thankful to him for providing me with an initial opportunity to conduct research, and helping me make the transition from a classroom to a laboratory so wonderfully. Thank you for your patience and zeal.

I want to thank Professor Alexi Arango for agreeing to be on my thesis committee and for his enthusiasm in a physics class where I discovered a fond appreciation for a new subject.

I also want to thank Professor Himali Jayathilake for her insightful suggestions and cheerful presence, Blanca Gonzalez for help with optical microscope, and Marian Rice for help with the SEM.

I was very lucky to work on this project alongside my talented student-mentor Lien Nguyen. She not only taught me my initial experimental procedures, but also crucially contributed in this project's completion. Additionally, I would like to thank all of my current and former lab members, each of whom have inspired me in this endeavor with their passion, intelligence, and kindness. Tarnuma, Lizzie, Bhanushee, Ye, Linda, and Kelly, thank you for your company.

To Suraj, Arati, Prarthana, Sahara, Pratistha, and Pavlina—thank you for your friendship and generosity.

I dedicate this thesis to my parents and siblings, for teaching me perseverance and giving me the courage to follow my heart.

LIST OF FIGURES AND TABLES

TABLE OF CONTENTS

ABSTRACT

While polydimethylsiloxane (PDMS) has many uses in analytical, biomedical, and electronic systems, its hydrophobicity hinders some of its applications by causing incompatibility with aqueous media. Specifically, this can cause great difficulties to the polymer's applications in bioengineering, as most biological systems are water-based. A direct and simple approach of surface adsorption is successful in hydrophilizing PDMS substrates.

In this research, surface hydrophillization of PDMS was carried out by adsorption of poly(vinyl alcohol) (PVOH, 99% hydrolyzed, M.W. = 89-98 kDa) from aqueous solution. PDMS of different molecular weights, from 2 kDa to 116 kDa, were covalently attached to silicon wafer substrates. All the substrates were characterized using ellipsometry, contact angle goniometry, and atomic force microscopy before and after each step.

Adsorbed PVOH thin films were only continuous on PDMS layers of 2 kDa and showed "dewetted" morphologies, such as honeycomb structures and fractal features, as the underlying PDMS molecular weight increases and decreases. The instability of the adsorbed PVOH thin films is likely caused by surface chemical and/or physical "defects". PVOH morphologies on various PDMS substrates are determined by the density and extent of defects in different PDMS substrates, and/or the molecular weights (flexibility) of PDMS chains. Lower molecular weight PDMS are most easily hydrophilized by adsorbed PVOH as indicated by the low receding contact angle values. Higher molecular weight PDMS have incomplete coverage of PVOH, giving rise to high advancing contact angle values.

In-situ imaging confirms that various PVOH morphologies are formed upon exposure to air, not in solution, and that PVOH desorption is minimal. The unique structural features of adsorbed PVOH thin films are likely the direct result of PVOH crystallization upon dehydration and are dependent on surface defects.

I. INTRODUCTION

1.1 Motivation for the project: creating a long-term hydrophilic surface

Polydimethlysiloxane (PDMS) is used in rapid prototyping of microfluidic devices due to its numerous advantageous properties. The polymer's ease of fabrication, low cost, biocompatibility, elastomeric quality, and optical transparency are properties that give it an upper hand in the manufacture of microfluidic devices.[1,2] Some applications utilizing microfluidic devices include polymerase chain reaction[3], DNA microarrays[4], capillary electrophoresis[5], stable droplet[6] and bubble formation[7], analysis of biological samples[8], and various other separation and point-of-care devices.

Despite the polymer's ubiquitous uses in various aqueous-based procedures, its intrinsic hydrophobic property remains a major impediment in its complete utilization. The advancing and receding water contact angles of PDMS surface are approximately $110^o/100^o$ (θ_A/θ_R) respectively; this means that the polymer is highly hydrophobic. The hydrophobicity of PDMS causes great difficulties to its applications in bioengineering, as most biological systems are aqueous. For instance, analysis of biological samples and chemical synthesis require hydrophilic surfaces. In order for capillary electrophoresis to work, there is the

need for some amount of surface wettability.[5] Stable droplet and bubble formations only work when the channel walls are wet for the flow of continuous phase fluid.[6, 7] Most importantly, many hydrophobic biomolecules easily adsorb nonspecifically onto the intrinsically hydrophobic polymer, thus hindering useful properties of PDMS substrates.[9]

However, such disadvantages can be suppressed by the implementation of novel surface modification techniques. The advantages of such techniques are two-fold: minimization of biomolecular adsorption and improvement in the hydrophilicity of the polymer.[9]

In an effort to hydrophilize PDMS substrates, various methods for treating PDMS surfaces have been implemented. Two primary strategies have been known to bring about PDMS hydrophilization: covalent modification and physical adsorption.[9] Covalent modifications can be achieved by introducing hydroxyl groups (-OH) onto PDMS surfaces. The hydroxyl groups can then be modified by a silanization process, where silane molecules are attached via siloxane (Si-O-Si) bonds. Depending on the type of silane used, various functional groups maybe attached onto PDMS surfaces.[10] In the past, oxygen plasma[11] and UV/ozone[12] have been used to make PDMS surfaces more hydrophilic by replacing surface methyl groups with silanol groups. A major drawback of such procedures, however, is that this modification is temporary because the polymer surface can

often regain its hydrophobicity in time in a process known as hydrophobic recovery.

An alternative process may also be adopted where an acidic solution containing hydrogen peroxide (H_2O_2) is pumped onto the PDMS surface creating silanol groups.[13] However, this process is not preferred as an excess of the acidity of hydrogen peroxide may lead to a loss in the optical transparency of PDMS.[9]

While physical adsorption is a simple one-step process in achieving hydrophilization of PDMS substrates, it also turns out to be unstable both thermally and mechanically. Such instability can be attributed to the weak interactions between the adsorbed molecules and the PDMS surface.

Is there then an easy and facile method to achieve long-term hydropilization of PDMS substrate without loss of the polymer's desirable properties? This project investigates hydrophilization of PDMS surfaces using adsorption of poly(vinyl alcohol) (PVOH) as a tool. Unlike previous cases of physical adsorption where the process was unstable due to weak interactions between the adsorbed molecule and the polymer, adsorption of PVOH on PDMS is a stable process. A two-stage process is known to occur during adsorption: firstly, a decrease in the interfacial energy due to the hydrophobic interaction between the inherently hydrophobic PDMS and the carbon backbone of PVOH, and secondly, a subsequent stabilization of the adsorbed layer due to crystallization of the polymer.[14] Adsorption of PVOH onto PDMS is a superior method over the studies

done in the past because of its simplicity, and its success in creating a long-term hydrophilic surface.

1.2 Polydimethylsiloxane: chemical structure and properties

Silicones are widely known today as polymers with an alternating silicon and oxygen single bonded backbone. Polydimethylsiloxane, the most common form of silicone, has two methyl groups attached to each silicon atom in its backbone.[15, 16] The structure of PDMS combines both organic (methyl) and inorganic (siloxane) groups, and is one of the most studied siloxane polymers.[17] Figure 1 shows the chemical structure of PDMS.

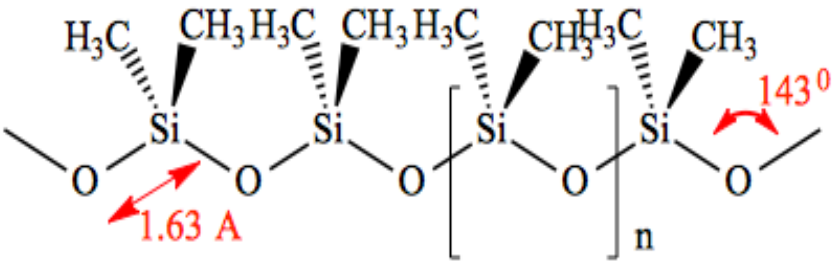

Figure 1. Chemical structure of polydimethylsiloxane, showing its large bond length, repeating unit, and bond angle.

There are three major structural properties of PDMS that allow for its rotational and vibrational degrees of freedom, such aspects are absent in carbon-

based substrates.[15] Firstly, the Si-O-Si bond angle of 143^{o} is much greater than the corresponding C-C-C bond angle of 109.5^{o}. Secondly, the Si-O bond (1.63 Å) is significantly longer than a typical C-C (1.53 Å) bond. And finally, the electro-negativity difference between silicon (1.9) and oxygen (3.5) atoms leaves Si-O bond with an ionic character of 51%. The first two properties of PDMS are the basis for some of the unique attributes of PDMS such as high flexibility and low glass transition temperature (-125 ^{o}C).[16] The last property, its high ionic character, allows chemical reactivity and permeability by water and oxygen, as well as thermodynamic stability.

A major distinction that needs to be established between polymers that are based on Si-O bonds rather than C-C bonds is their thermal stability, where the former exhibits much greater thermal stability.[15] The reason for this difference is two-fold: a greater bond dissociation energy of Si-O bonds (444 kJ/mol) compared to that of C-C bonds (346 kJ/mol), and yield of a solid SiO_2 in the case of silicon based substrates compared to carbon based substrates which yield a gaseous oxidation product of CO_2.[15]

With a glass transition temperature (T_g) of -125 ^{o}C, uncrosslinked PDMS exists as a liquid at room temperature. This means it does not undergo permanent deformation upon applying stress or strain and therefore exhibits elastomeric properties in its crosslinked form.[18]

The presence of methyl groups attached to the silicon atoms of its backbone contributes to the non-swelling characteristic of PDMS in aqueous media, however; this also gives rise to its inherent hydrophobicity. While properties of PDMS such as thermal stability, chemical inertness, non-toxicity, and biocompatibility are highly desirable, its hydrophobic nature brings forth challenges in biomedical devices required to be functional in aqueous environments.[18]

1.3 Introduction to poly(vinyl alcohol)

PVOH is a non-toxic polymer and has innumerable applications as emulsifiers, coatings, food-packaging materials, biomaterials, drug delivery systems, adhesives, surfactants, etc.[19]

Figure 2 shows the chemical structure of PVOH. PVOH is a white solid at room temperature and is water-soluble.[20] It is an unusual polymer in that it is atatic yet semi-crystalline.[21] PVOH is one of the most hydrophilic polymers with stable chemical properties, good dissolution, and strong adhesion.[22] It is a polymer of interest due to its many desirable properties, and can therefore be used for various pharmaceutical and biomedical applications.

The degrees of hydrolysis and polymerization affect the solubility of PVOH in water. It has been shown that PVOH solutions with high degrees of hydrolysis

have low solubility in water. Furthermore, the presence of acetate groups affects the ability of PVOH to crystallize.[23]

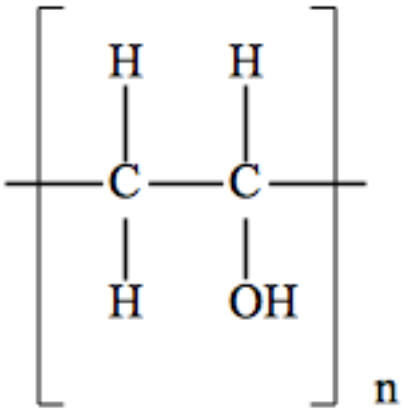

Figure 2. Chemical structure of a poly(vinyl alcohol) repeat unit.

Figure 3 shows solubility as a function of degree of hydrolysis for a PVOH of M_n = 77,000 Da at temperatures of 20 ^{0}C and 40 ^{0}C. The graph shows that the percentage of PVOH soluble in water is inversely proportional to its degree of hydrolysis. Hence, solubility will decrease as the degree of hydrolysis increases. This occurs because the residual hydrophobic acetate groups weaken the intermolecular and intramolecular hydrogen bonding of hydroxyl groups. It turns out that 70 ^{0}C and higher temperature is required in order for dissolution to occur.[23] PVOH has a melting point of 230 ^{0}C for the fully hydrolyzed grade and a melting point of 180-190 ^{0}C for its partially hydrolyzed grades.[24] Its glass transition temperature is 85 ^{0}C.[25] The low critical solution temperature (LCST) of PVOH is 97 ^{0}C. Above this temperature, the chains of the polymer become

hydrophobically associated or aggregated, leading to phase separation and the formation of agglomerates.[26]

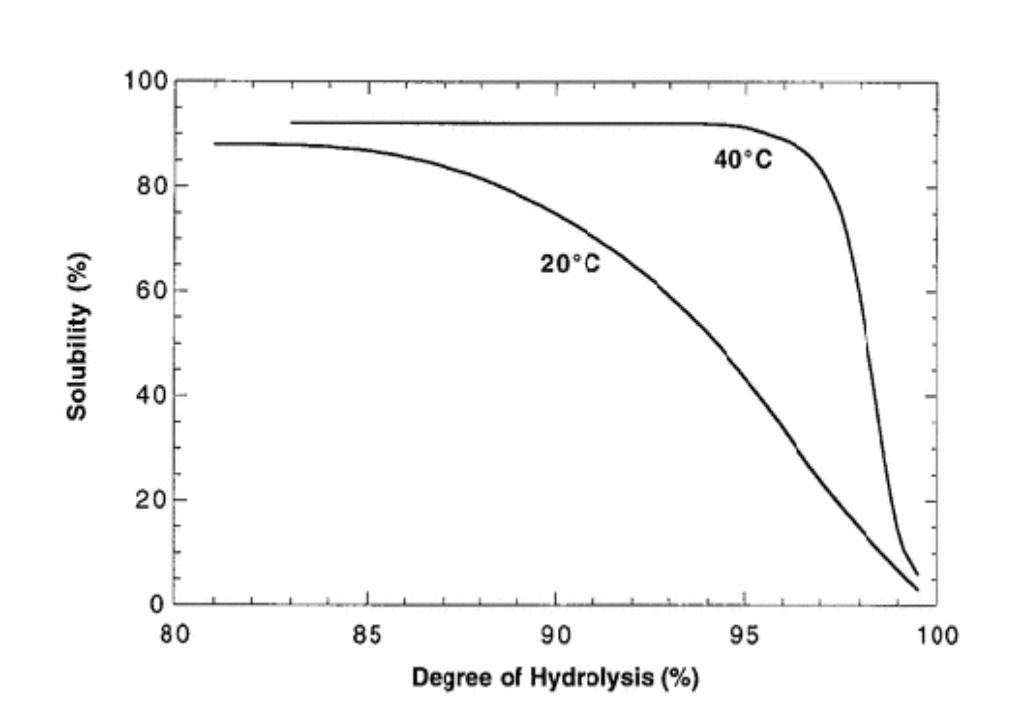

Figure 3. Percent of solubility as a function of degree of hydrolysis for a PVOH of M_n = 77,000 at 20 ^{0}C and 40 ^{0}C.[23]

An interesting aspect of making PVOH is that rather than it being made from the polymerization of its precursor single unit monomer vinyl alcohol, it is prepared by first polymerizing vinyl acetate, and then hydrolyzing poly(vinyl acetate) to PVOH. This is because the keto form of the tautomer of vinyl alcohol is favored over its enol form. Figure 4 shows the tautomerization of vinyl alcohol. Vinyl alcohol, in its enol form is not as stable to undergo a polymerization

reaction. And so, vinyl acetate is used as the initial monomer to make poly(vinyl alcohol).[19]

As shown in Figure 5, the conversion of poly(vinyl acetate) to PVOH is done via the addition of methanol and an alkaline catalyst such as sodium hydroxide.[19]

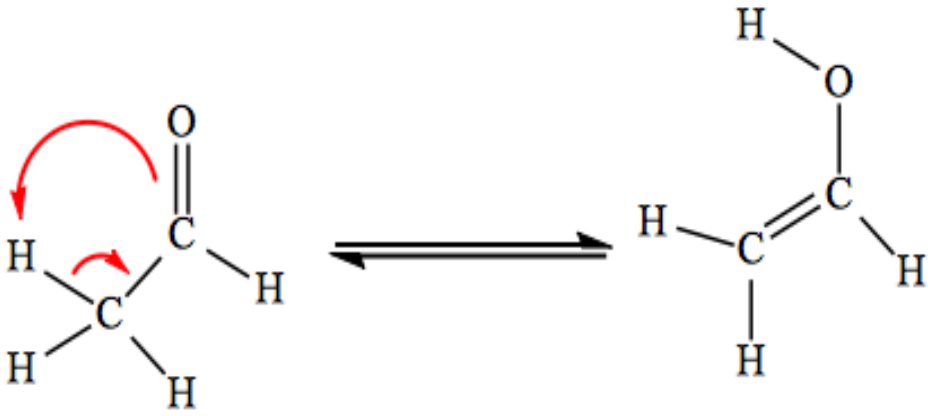

Figure 4. Tautomerization of vinyl alcohol; the reaction is favored to the left with the keto form dominating the equilibrium.

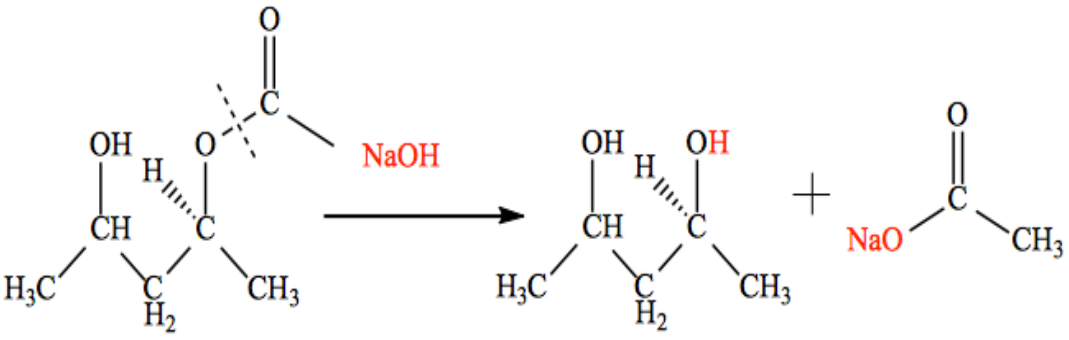

Figure 5. Hydrolysis of poly(vinyl acetate) to poly(vinyl alcohol) in the presence of NaOH.

1.4 PVOH adsorption and its driving forces

A direct and simple approach for making PDMS surfaces more hydrophilic is via surface adsorption.[27]A way to achieve this is by adsorbing PVOH onto PDMS surfaces.

PVOH has been shown to adsorb irreversibly onto many different hydrophobic solids by it being surface-active at a hydrophobic surface/water interface.[28] Furthermore, it has been hypothesized that the surface of the PVOH thin films reconstruct upon drying to a structure that is different from the polymer that is in contact with water.[28]

The driving forces attributing to the spontaneous PVOH adsorption are hydrophobic interactions between the PDMS chain and PVOH carbon-based backbone followed by a subsequent crystallization.[14] The hydrophobic interactions between the two polymers induce the release of water from the solid-liquid interface, followed by a subsequent crystallization of PVOH polymer chains at the interface.[28] Thus the driving force for the hydrophobic interactions arises from an increase in entropy of the water.

Figure 6 shows a Langmuir curve, which is quantitatively described by the Langmuir equation. The Langmuir curve relates the coverage or adsorption of

molecules on a solid surface to the concentration of the medium above the solid surface, at a fixed temperature.[29] The Langmuir equation is as follows:

$$\Theta = \frac{\alpha P}{1+\alpha P}$$

Where, Θ is the fractional coverage, P is the concentration (or pressure), and α is a constant.[29]

The constant α is known as the Langmuir adsorption constant and it increases as the binding energy of adsorption increases and as the temperature decreases. In Figure 6, the value of the constant α increases from blue (bottom curve) to brown (top curve). Therefore, adsorption increases as a function of temperature.[29]

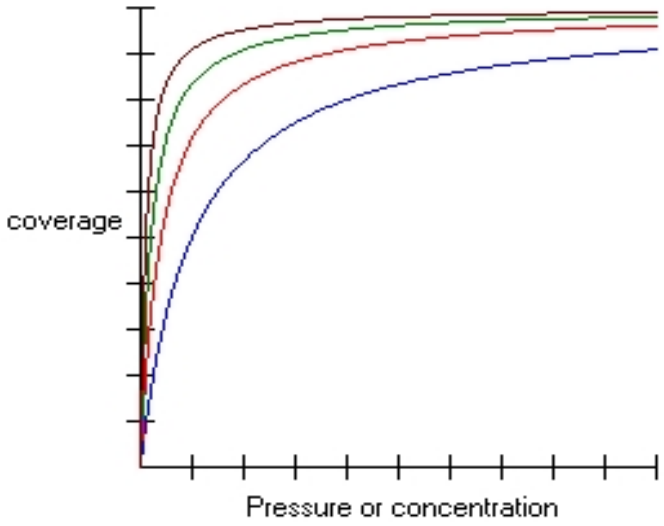

Figure 6. The Langmuir curve showing fractional coverage vs. concentration.[29]

1.5 Understanding dewetting

In this research, we strive to understand a "dewetting-like" phenomenon that occurs after the adsorption of PVOH onto PDMS. Dewetting is a spontaneous phenomenon where a liquid thin film on a surface rearranges itself into an ensemble of separated objects.[30]

Dewetting can be ascribed to the interplay of unfavorable surface interactions and attractive intermolecular forces. Dewetting is a spontaneous withdrawal of a liquid film from a hostile surface and can be viewed as the opposite of spreading of a liquid film on a substrate.[31, 32, 33]

Figure 7 shows the three different types of dewetting mechanisms. The first type, dewetting by nucleation, occurs in the case of thicker films, where the gravitational forces are dominant over the intermolecular forces due to the larger thickness of the films. Overall, the film is relatively stable, and so, dewetting by nucleation is initiated by the nucleation of holes at defect sites.[30] In spinodal dewetting, the films are so thin that the gravitational forces are negligible compared to the intermolecular forces. Thus, attractive long-range forces cause the film to be unstable, and break apart into an array of droplets.[30] The third type of dewetting known as Ostwald ripening occurs when heat is supplied to isolate droplets that rupture due to the instability of thin films to merge together, grow, and finally crystallize.[30]

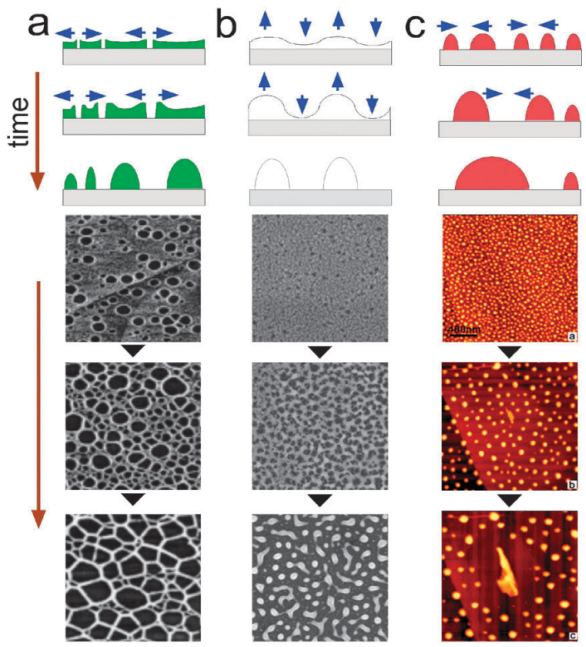

Figure 7. Schematic representation of different dewetting types. **a)** Dewetting by nucleation, growth and coalescence of holes. **b)** Spinodal dewetting. **c)** Dewetting by Ostwald ripening followed by crystallization.[30]

Before trying to understand the phenomenon of dewetting, two main types of wetting regimes must first be understood. Two main sectors of wetting are total and partial wetting. Figure 8 shows the two different wetting mechanisms. These can be differentiated by the spreading parameter S.[30] The spreading parameter can be expressed as:

$$S = [E_{sub}]_{dry} - [E_{sub}]_{wet} = \Upsilon_{S\text{-}A} - (\Upsilon_{S\text{-}L} - \Upsilon_{L\text{-}A}),$$

Where, the three coefficients Υ are the surface tensions at the solid-air, solid-liquid, and liquid-air interfaces, respectively.[30] $[E_{sub}]_{dry}$ is the surface energy per

unit area of the dry substrate and $[E_{sub}]_{wet}$ is the surface energy per unit area of the wet substrate.

When the wetting parameter S is positive, the liquid spreads completely forming a contact angle of $\theta_E = 0$.[30] In the case of partial wetting, S is negative, and the liquid forms a hemi-spherical cap on the substrate surface with θ_E with a positive value between 0 and 108^0.[30] When partial wetting occurs, films are either metastable or unstable and dewet below the critical thickness h_c, where h_c can be expressed as:

$$h_c = 2\sqrt{\frac{\gamma}{\rho g}} \sin\left(\frac{\theta_E}{2}\right)$$

Where, h_c is in the order of millimeter, g is the acceleration of gravity, ρ is the liquid density, and γ is the interfacial energy.[30]

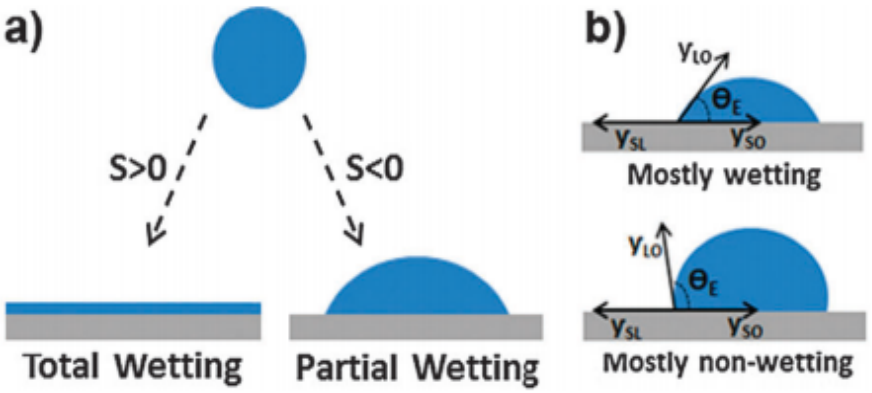

Figure 8. a) Two different types of wetting regimes: Total wetting with a positive spreading coefficient and partial wetting with a negative spreading coefficient. **b)** Contact angles in two partial wetting scenarios: mostly wetting with contact angles less than 90° and mostly non-wetting with contact angles greater than 90°.[30]

Applications of dewetting. Dewetting can be useful in many industrial processes where a fast drying surface is required. Examples include aviation, metallurgy, dishwater detergents, and as substitutes to expensive lithographic processes.[34] Nonetheless, dewetting is considered to be undesirable in industry due to its most obvious property: break-up of liquid into an array of small droplets. This can be undesirable in cases where a smooth coating is required. Understanding of the dewetting phenomenon, however, has led to the ubiquitous application of dewetting in many industrial processes. Examples of these include fabrication of large ordered structures, production and reproduction of molds as patterns, and its usage in various electronic applications as field effect transistors and resists.[34]

One such study reported an easy and facile method to make grafted polymer brushes using the dewetting theory.[35] Polymer brushes are widely used as a reliable way to modify the functionality of surfaces. Such functionalities include the polymer surface's wettability, biocompatibility, and resistance to corrosion and friction.[36, 37] Figure 9 summarizes the process of forming grafted polymer brushes using the dewetting mechanism. In step 1, a film of micro initiator is spin-coated on top of a polystyrene (PS) film.[35] In step 2, the micro initiator film

dewets upon thermal annealing and forms holes.[35] In step 3, the poly(poly(ethylene glycol) methyl ether methacrylate) chains are grafted, but only onto the micro initiator films.[35] This way, a patterned brush is produced, which is able to adsorb only within the PS holes.[35] Such polymer brushes have ends that are able to selectively attach to only certain types of cells; this can be fundamental in the formation of tissues in vitro and in bio-sensing. The patterning of polymer brushes, especially in biomedical applications, has been carried out in the past using rather complex methods such as micro-contact printing and scanning probe microscopy-assisted writing.[38-40] Dewetting is favored over lengthy lithographic scanning procedures due to it being a cheaper and faster method.[35]

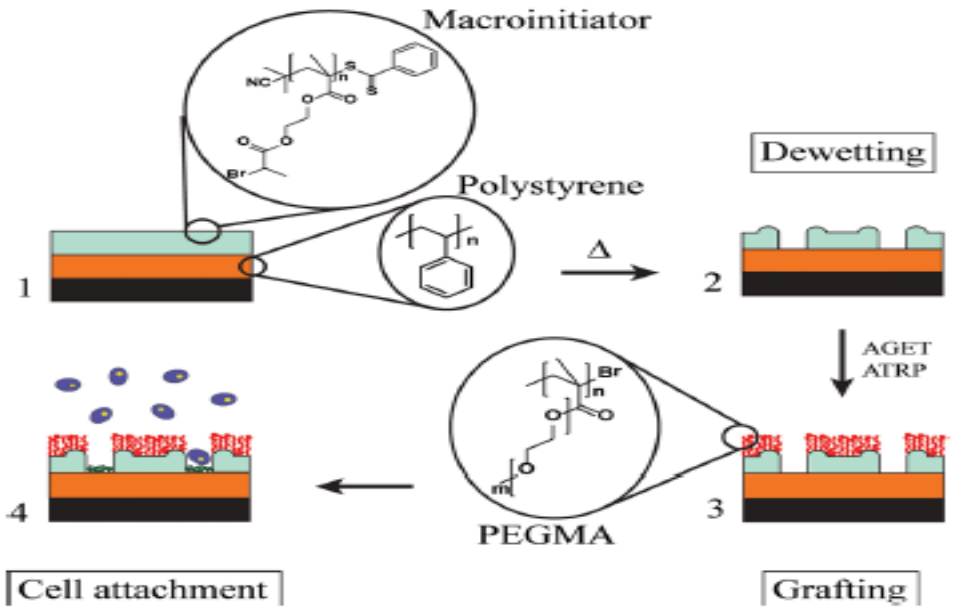

Figure 9. A facile one-step method polymer brushes using dewetting.[35]

Role of dewetting in biological systems. The dewetting phenomenon is important in biological systems at the solid-liquid interfaces such as: *in-vitro* experiments, biosensors, and arrays.[41] For example, the stability in the conformations of proteins and nucleic acids can be largely attributed to the interplay of hydrophobic and hydrophilic forces.[42] This means that proteins at surfaces experience conformational changes, which may be used to change a protein's surface energy and modify the intermolecular interactions between them.[43] So depending on the interaction between proteins, either aggregation or segregation of protein pairs can occur. This induces the formation of either monolayers (wetting-like) or isolated nanostructures (dewetting-like). [30] Patterning of cell-adhesive proteins on hydrophobic surfaces is also important in implants and tissue reconstruction.[44-46]

1.6 An in-depth study of dewetting: two main rupture mechanisms

On the one hand, a defect-free and smooth coating is desired in most cases. An application of this includes stable lithographic resists.[48] On the other hand, the basic rules that constitute dewetting can be used and applied to other systems so that general rupture mechanisms can be inferred.[49]

A "dewetting-like" phenomenon has been shown to give rise to the various PVOH morphologies observed on PDMS substrates of different molecular

weights after adsorption. Figure 10 shows the various morphologies formed on different molecular weights of PDMS substrates. A former member of the lab, Lien Nguyen, obtained the images taken with optical microscope (top row) and AFM (bottom row) shown in Figure 10.

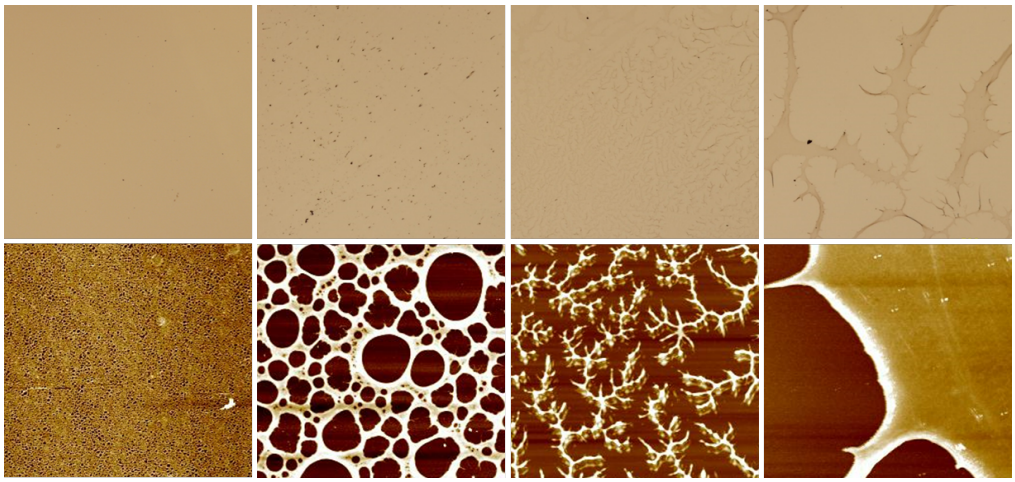

Figure 10. Macroscopic and microscopic morphologies of features formed by PVOH adsorption. Top row, left to right: 1000 μm × 1000 μm optical microscope images of $PDMS^{2000}$, $PDMS^{9430}$, $PDMS^{17250}$, and $PDMS^{49350}$. Bottom row, left to right: 10 μm × 10 μm AFM images of $PDMS^{2000}$ (height scale bar = 10 nm), $PDMS^{9430}$ (20 nm), $PDMS^{17250}$ (50 nm) and $PDMS^{49350}$ (50 nm).

Although what we see is different from the conditions in which dewetting has been observed in the past, the similarities in morphologies between what we see and the dewetting phenomenon means that the possibility of a "dewetting-like" mechanism in this case must also be considered. Unlike the case of dewetting where a certain liquid including molten polymer interacts with a solid substrate, dehydration of adsorbed PVOH thin films occur upon exposure to air. The driving

force is the instability of the thin film and crystallization as a result of dehydration.

To begin with, we must understand that a film can either be stable, meta-stable or unstable. The effective interface potential $\varphi(h)$ must first be defined: $\varphi(h)$ is the excess free energy per unit area necessary to bring two interfaces (solid-liquid and liquid-gas) from infinity to a certain distance h, the thickness of the liquid film.[48] As shown in Figure 11, as h approaches infinity $\varphi(h)$ approaches 0.[48] This indicates that a film with infinite thickness is stable. Curve 1 in Figure 11 shows that when $\varphi(h)$ is positive, the film is called stable. Curve 2 shows that when the second derivative of φ with respect to the film thickness is negative, i.e $\varphi''(h_0)$ is negative and h_0 is the initial thickness of a homogeneous film, the film is called unstable.[48] Curve 3 shows that the film is unstable for small film thicknesses where $\varphi''(h_0)$ is negative, and metastable for larger film thicknesses, where $\varphi''(h_0)$ is positive.[48] The h* in Figure 11 represents nucleation or defect sites, this is the point at which the films can undergo dewetting by heterogeneous nucleation.

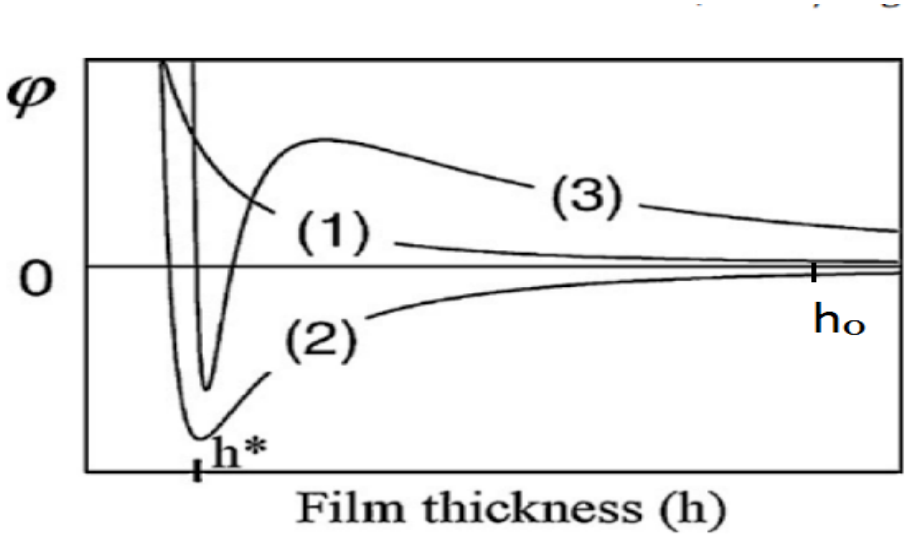

Figure 11. Effective interface potential $\varphi(h)$ as a function of film thickness h for stable (1), unstable (2), and metastable (3) films.[49]

Dewetting is characterized by the formation of holes, their growth, and coalescence, finally leading to a set of droplets on the substrate.[49] In the metastable case ($\varphi''(h_0) > 0$, curve 3 in Figure 11), the film ruptures due to a nucleation process initiated either by defect sites or heat. A consequence of this is that the holes appear at random locations. Figure 12 shows an AFM image of dewetting by nucleation.

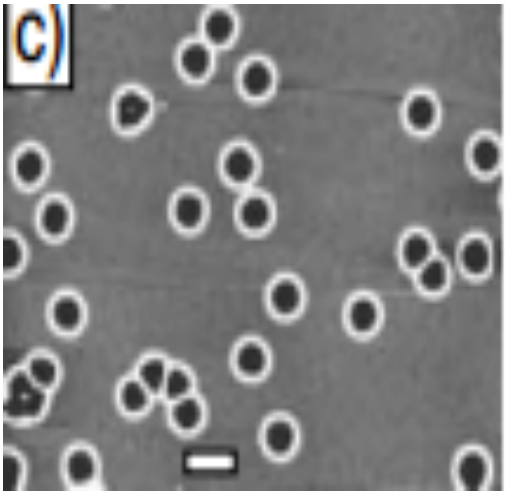

Figure 12. AFM image of a polystyrene (2k) film showing dewetting by nucleation.[49]

In contrast, an unstable film ruptures spontaneously via a spinodal dewetting mechanism ($\varphi''(h_0) < 0$, curve 2 in Figure 10).[49] Instability arises due to a small fluctuation in the system parameter.[49] The capillary waves are spontaneously amplified and the fluid advances to a rim, which can grow.[49] A consequence of this is that the holes appear at regular distances from each other. Figure 13 shows an AFM image of an unstable film undergoing spinodal dewetting. Since dewetting is a process related to film thickness, AFM is the most ideal tool to obtain topographical images of the sample, as well as obtain some of the surface properties like electric, magnetic, and elastic.[50]

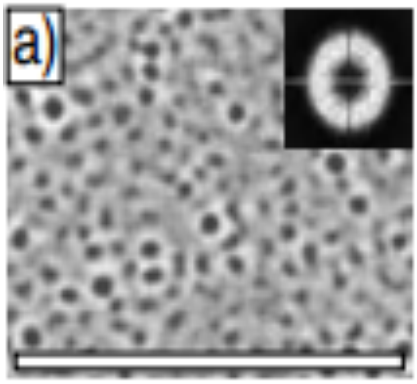

Figure 13. AFM image of a polystyrene (2k) film showing spinodal dewetting.[49]

1.7 Atomic force microscopy and three imaging modes

Atomic force microscopy is a widely used high resolution imaging technique, which has gained popularity in recent years. It consists of a cantilever with a sharp tip that is used to scan sample surface.[51] Information about the morphology of a surface is gathered by the cantilever tip, which deflects upon interaction with the sample surface. A feedback loop is created in order to adjust the tip to sample distance. As shown in Figure 14, as the cantilever is displaced due to its interaction with the surface, the reflection of the laser beam will also be displaced on the surface of the photodiode.[51]

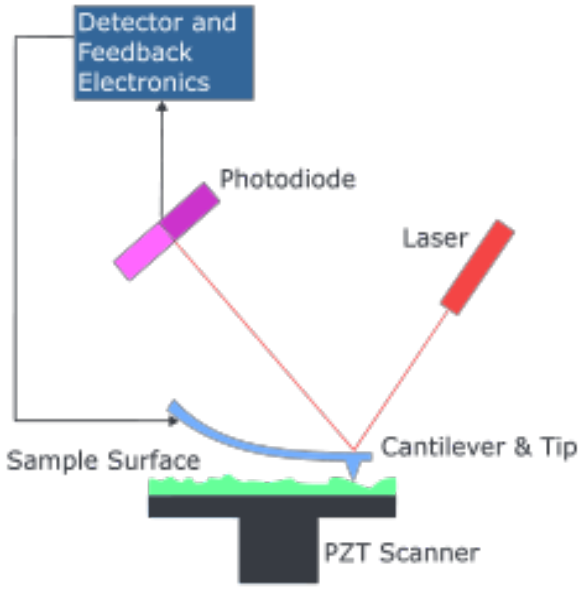

Figure 14. A block diagram of an atomic force microscope.[52]

AFM can be operated in three imaging modes. These are contact mode, non-contact mode, and tapping mode. In contact mode, the tip is dragged across the surface of a sample resulting in a topographical map of the surface.[53] A major disadvantage of this mode is the presence of adhesive forces between the tip and the surface, which can cause substantial damage to the sample and the cantilever, thereby creating artifacts.[53] A way to avoid this problem is by implementation of non-contact mode. In this mode, the tip is held at a small distance above the sample. However, its problems can manifest in low resolution. A third and the most efficient type is the tapping mode. Figure 15 shows an AFM image obtained using the tapping mode.

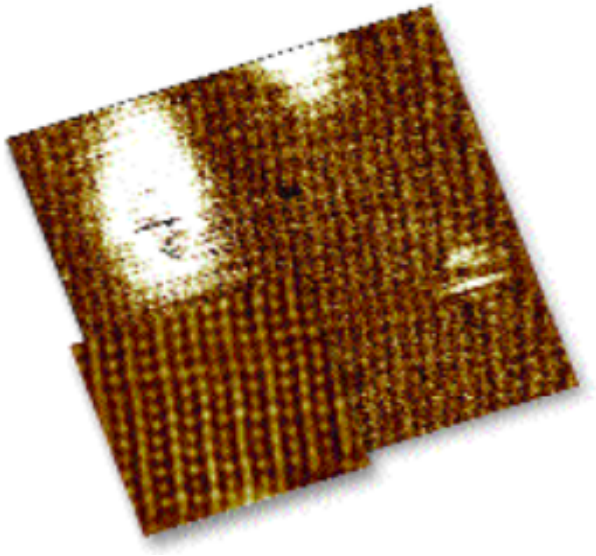

Figure 15. Tapping mode image of purified collagen monomers.[53]

Tapping mode is able to conveniently scan a surface by allowing the tip in contact with the surface to provide high resolution, and then lifting the tip off to avoid any damages resulting due to dragging. This motion can cause an oscillation of the AFM tip.[56] In tapping mode, a constant feedback loop is maintained by the cantilever oscillation amplitude. This method can especially be useful in the case of soft samples as the tapping mode prevents sample surfaces from getting damaged due to the oscillation amplitude overcoming any tip-sample adhesion.[53]

1.8 Geometry and morphology of fractals

Information about fractal geometry is useful in our investigation of fractal morphologies of PVOH on PDMS substrates. The term fractal was coined by the French-American polymath Benoit Manderbolt about four decades ago and it is derived from the Latin word fractus, meaning broken.[54] Figures 16 and 17 illustrate the major difference between a fractal and a non-fractal object. Upon magnification of a non-fractal object, no new features are revealed. Magnification of a fractal, however, reveals finer features that are in turn similar to the larger features.[54]

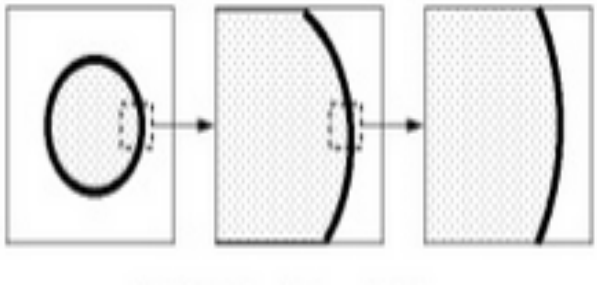

Figure 16. A non-fractal object.[54]

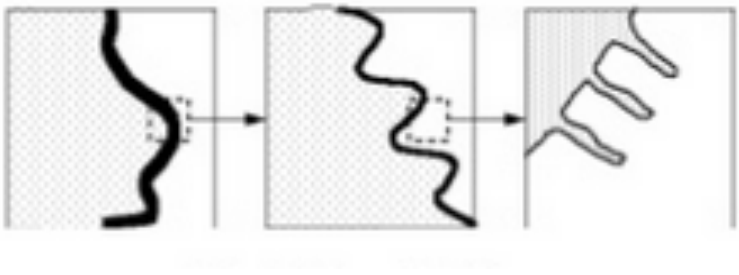

Figure 17. A fractal object.[54]

In the real world, many different objects can be classified as fractals based on this property. Some examples of fractals occurring naturally are neurons, tree branches, and snowflakes.[55] Fractals have extensive uses in the modeling of the universe, data compression, study of music, weather forecasting, special effects in computer graphics, medical imaging, and signal processing.[55]

Copious amounts of work have been done in order to model fractals. In the 1980s, Witten and Sanders proposed the diffusion limited aggregation (DLA) model (Figure 18). The model assumes the kinetic growth of clusters involving random walk diffusion and irreversible addition of new particles to the edges of existing, stationary features with diffusion as the rate-limiting step.[56] In the DLA model, the fractal morphologies grow by the successive addition of particles, so the clusters must be formed *in-situ* and their growth must be attributed to Brownian motion.[56]

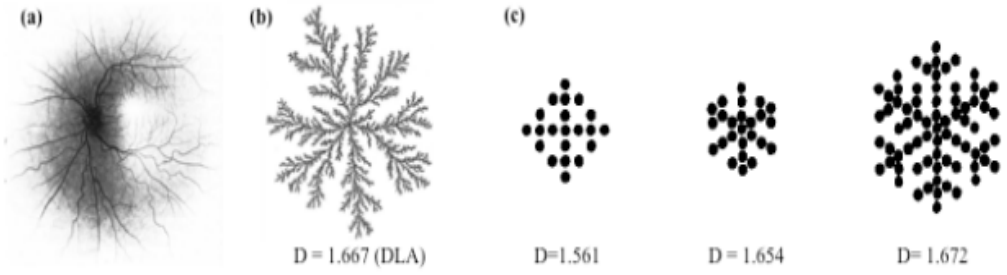

Figure 18. a) A fractal structure formed by a blood vessel around a retina.[57] b) A computer simulated 2-dimensional lattice as predicted by the DLA model. c) Examples of 2-dimensional lattice fractal structures.[58]

1.9 Project goals and objectives

In this project, investigation of the adsorption of PVOH on PDMS layers of varying molecular weights covalently attached to silicon wafers was carried out. Our investigation confirms that PVOH adsorbs on PDMS, and in doing so, forms a variety of macroscopic and microscopic features. Features range from continuous membranes to fractal morphologies.

The hypothesis of this project is that the morphology of the adsorbed PVOH changes as a function of molecular weight of PDMS. More specifically, the morphology of the adsorbed PVOH on PDMS changes from continuous films, to a combination of honeycomb and fractal morphologies, to exclusively fractal morphologies, as the molecular weight of PDMS increases. Understanding the causes behind the different PVOH morphologies across a range of PDMS molecular weights will help us understand adsorption.

Using *in-situ* imaging, the project aims to understand whether fractals form upon exposure to air (*ex- situ*) or in solution (*in-situ*). Some type of a "dewetting" mechanism seems to be the likely phenomenon behind changes seen in the morphology of the PVOH films. The methods of rupture of PVOH films onto the different molecular weights of PDMS were also investigated. On lower molecular weight PDMS substrates, continuous films are a consequence of "spinodal dewetting". As molecular weight of PDMS increases, there is an increase in the number of defect sites of the substrate. Such defect sites can bring about

instability in the films and initiate “dewetting by nucleation”. This “dewetting” gives rise to the honeycomb structures, transitional morphologies, and fractal structures that are observed.

Furthermore, this project aims to investigate the interplay of factors that ascribe to the driving forces involved in adsorption. Namely, two primary factors are known to affect adsorption, these include: 1) hydrophobic interactions and 2) crystallization of PVOH on the substrate. Once a paradigm for the PVOH morphologies on PDMS substrates of varying molecular weight was established, solubility tests of adsorbed PVOH films on a single type of PDMS substrate were carried out. This provides hints toward the formation mechanism of fractals upon drying (*ex-situ*).

Measurement of crystallinity of PVOH films adsorbed onto PDMS substrates will be a vital future step for furthering our understanding of the unique structural morphologies formed after adsorption. Additionally, we hope to be able to control the surface morphologies (shape and size of fractals, types of honeycomb structures, coverage of continuous films, etc.) of a single type of a PVOH adsorbed PDMS with the knowledge gained from solubility and kinetics tests. Knowledge of whether PVOH desorbs back into water would reveal whether or not adsorbed PVOH is crystalline in nature and soluble in water.

In our investigation of the hydrophilization of PDMS using PVOH, we have successfully established standard experimental procedure, achieved

reproducibility, and optimized conditions to create a long-term hydrophilic substrate.

II. MATERIALS AND METHODS

2.1 Materials and Instrumentation

Materials. Silicon wafers were purchased from International Wafer Service, Inc. DMS-T12 (M.W. = 2,000 Da), DMS-T22 (M.W. = 9,430 Da), DMS-T25 (M.W = 17,250 Da), DMS-T35 (M.W. = 49,350 Da), and DMS-T46 (M.W. = 116,500 Da) were purchased from Gelest, Inc. Poly(vinyl alcohol) (89-98 k, 99+% hydrolyzed) was purchased from Sigma-Aldrich, Co. Water was purified using a Milli-Q Biocel system (Millipore Corp, resistivity ≥ 18.2 MΩ/cm). Toluene, acetone, and ethanol were purchased from Fisher Scientific, Inc.

Instrumentation. All silicon wafers were oxidized in a Harrick plasma cleaner PDC-001 (Harrick Scientific Products, Inc.) prior to drop-casting. Drop-casted wafers were heated in the model 150/Timer heater (J-KEM Scientific, Inc.). Dynamic light scattering measurements were carried out using Malvern Zetasizer Nano-S equipped with a 4mW He-Ne laser (λ = 632.8 nm) to determine the size of PVOH chains in solution. Refractive indices of PVOH (n = 1.520) and water (n = 1.330), and viscosity of water (η = 0.8872) at 25 ^{o}C were assigned. The measurements obtained have ~ 5% relative error. Precision 51221126 Gravity Convection Lab Oven (Thermo Fisher Scientific, Inc.) was used for drying silicon wafers. Olympus BX51 optical microscope in the reflective mode was used to obtain macroscopic images of substrates. Thickness measurements were carried out using an LSE Stokes Ellipsometer (Gaertner Scientific Corp.) equipped with a

1 mW He-Ne laser (wavelength 632.8 nm). Contact angles were measured using a NRL C.A 100-00 goniometer (Rame-Hart Instrument Co.) with a Gilmont Syringe (Gilmont Instrument Co.) attached to a 24-gauge flat-tipped needle. Surface topographies were imaged using a Veeco Metrology Dimension 3100 Atomic Force Microscope (Veeco Instruments Inc.) in tapping mode with a Veeco silicon tip. *In-situ* imaging of PVOH adsorption on PDMS substrates was carried out using a 10× Nikon water immersion lens and a Q-Imaging QICAM camera attached to a Nikon eclipse 50 i optical microscope.

2.2 Methods

Preparation of clean silicon wafers. Silicon wafers were cut into 1.2 × 1.5 cm rectangular pieces, rinsed with distilled water, and dried with compressed air to remove impurities such as dust particles. The wafers were then placed in an oven to dry at 110 ^{o}C for 30 min. Moreover, in order to remove any organic contaminants, dried wafers were placed in an oxygen plasma reactor for 15 min at ~300 mtorr after flushing with oxygen gas three times for 30 s each time.

Drop casting PDMS onto clean wafers. Each clean silicon wafer was placed inside an individual clean scintillation vial. 100 μL of PDMS of varying molecular weights was drop cast onto each wafer using a micro-pipette. The vials were tightly capped after drop-casting, and placed inside slots of the heater at 100 ^{o}C for 24 h.

Rinsing drop casted PDMS substrates. After 24 h, the vials were removed from the heater. Each wafer was rinsed with toluene, acetone, and Milli-Q water in that respective order. Each wafer was rinsed 3× on top and 3× on bottom with each solvent; the rinsing procedure was repeated after changing the location where the tweezers were held. The wafers were dried under a stream of nitrogen gas and placed in a desiccator for overnight drying.

Preparing poly(vinyl alcohol) solution. In order to make a 0.1 wt% PVOH solution, 0.1 g of PVOH powder was weighed and added to a clean 120 mL Nalgene bottle. A magnetic stir bar and 100 g of Milli-Q water were added to the bottle. Meanwhile a hot water bath containing a stirrer was set up. The bottle was clamped so that it remained immersed in water and the water level of the outer water bath was kept at the same level as that of the PVOH solution inside the bottle. A thermometer was clamped and immersed in the water bath to keep record of the temperature. The bottle was heated at a temperature of 88-94 ^{o}C for 3 h. It was critical that the temperature did not exceed 95 ^{o}C, since 97 ^{o}C is the lower critical solution temperature (LCST) of the polymer above which the polymer chains become hydrophobically associated leading to phase separation and the formation of agglomerates.[26] Upon completion of heating, the solution was allowed to cool in the water bath under stirring overnight. Measurement of PVOH size in solution using the dynamic light scattering equipment commenced from the following day until PVOH size was finally stabilized. When stable, the

average hydrodynamic diameter of PVOH chains is approximately 18 nm by intensity and 14 nm by volume.

Adsorption of PVOH onto PDMS. Four silicon wafer samples grafted with PDMS with shiny side up were inserted into a wafer holder, which was was placed inside a Schlenk tube containing a stir bar. 15 mL of PVOH solution was slowly poured into the Schlenk tube from the side without directly contacting the wafers until all four wafers were completely submerged in PVOH. The Schlenk tube was then covered with a piece of parafilm. PVOH adsorption was allowed to take place for 15 min or 24 h at room temperature. After adsorption, 30 mL of Milli-Q water was added to the Schlenk tube. The mixture of PVOH and Milli-Q water was stirred for 1 min. Within the next minute, 30 mL of the mixture was pipette out. Addition of water and removal of solution were repeated for a total of 6 times. The 6^{th} addition, however, was not pipetted out. The wafer holder was taken out after the dilutions and the wafers were placed in a desiccator overnight after removing excess liquid.

Solubility tests. Three solubility tests were conducted in order to test the effects of different degrees of drying on the solubility of the adsorbed PVOH films. 1) Wafers were adsorbed for 24 h in 15 mL of PVOH. Dilutions were done 6× with 30 mL of Milli-Q water. After the 6^{th} removal of solution, the wafer holder was left inside the Schlenk tube for an additional 24 h. The wafer holder was taken out after 24 h and the wafers were placed inside a desiccator overnight

after removing excess liquid. 2) Wafers were adsorbed for 24 h in 15 mL of PVOH. Dilutions were done 6× with 30 mL of Milli-Q water. The wafer holder was lifted and transferred into an empty Schlenk tube, to which 15 mL of Milli-Q water was added. The wafer holder was taken out after 24 h and the wafers were placed in a desiccator overnight after removing excess liquid. 3) Wafers were adsorbed for 24 h in 15 mL of PVOH. Dilutions were done 6× with 30 mL of Milli-Q water. The wafers were taken out and dried in a desiccator for 24 h. After 24 h, the wafers were placed inside a Schlenk tube, to which 15 mL of Milli-Q water was added. The wafer holder was taken out after 24 h, and the wafers were placed in a desiccator overnight after removing excess liquid.

Re-adsorption. Wafers that were adsorbed with PVOH for 24 h and dried in a desiccator overnight were adsorbed in PVOH solution again for 24 h. The solution was diluted 6× before the samples were removed and placed in a desiccator overnight.

In-situ optical microscopy imaging. The processes of PVOH adsorption and desorption were captured *in-situ* using time-lapse imaging over a 24-hour period. For the adsorption studies, silicon wafers grafted with $PDMS^{2000}$ and $PDMS^{49350}$ were secured into separate polypropylene dishes using double stick tapes. Polymer aggregates and dust particles were removed from the PVOH solution using a 0.2 μm Nylon filter. The filtered PVOH solution was slowly added to the dish using a 10 mL syringe so that the PVOH solution completely cover each

wafer and that solution level filled approximately 90% of the dish. The dish was positioned such that the edge of the wafer could be focused while the 10× Nikon immersion lens dipped into the solution. Once the wafer was focused, time-lapse images of adsorption were captured for 24 h with one image being captured every hour. For the desorption studies, each of the $PDMS^{2000}$ and $PDMS^{49350}$ wafers adsorbed with PVOH was secured in a polypropylene dish. Milli-Q water was poured into each dish to about 90% full. Time-lapse images of desorption were captured for 24 h with one image being captured every hour. To minimize water evaporation, a plastic cover was placed over the dish during imaging.

III. RESULTS AND DISCUSSIONS

3.1 Mechanisms for the formation of different PVOH morphologies on PDMS substrates due to *ex-situ* "dewetting"

Figure 19 shows AFM images of five different molecular weights of PDMS grafted on silicon wafer substrates. The AFM root-mean-square (rms) roughness value of PDMS increases upon increasing molecular weights of PDMS. This is because the surface of PDMS gets rougher as molecular weight of PDMS increases.

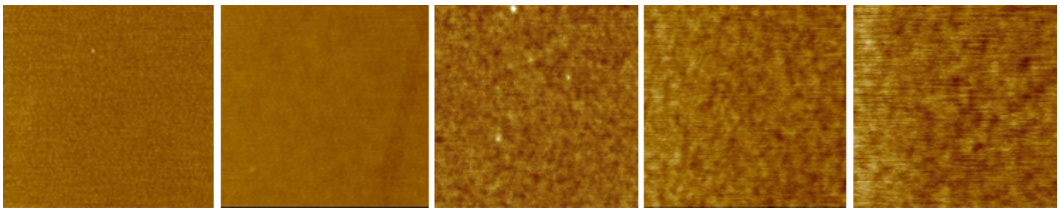

Figure 19. AFM images of PDMS on silicon wafers (scan size: 2.5 μm × 2.5 μm, height scale: 10 nm): T12 (M.W. = 2,000 Da, rms = 0.2), T22 (M.W. = 9,430 Da, rms = 0.3), T25 (M.W. =17,250 Da, rms = 0.3), T35 (M.W. = 49,350 Da, rms = 0.4), and T46 (M.W. = 116,500 Da, rms = 0.5) (from left to right).

Figure 20 shows AFM images of changes in PVOH morphologies as molecular weight of PDMS varies from 2,000 Da to 116,500 Da. A range of macroscopic and microscopic morphologies was observed in adsorbed PVOH. Continuous films and honeycomb structures were more common in lower molecular weight PDMS substrates. Small and large fractal morphologies were more common on higher molecular weight PDMS substrates.

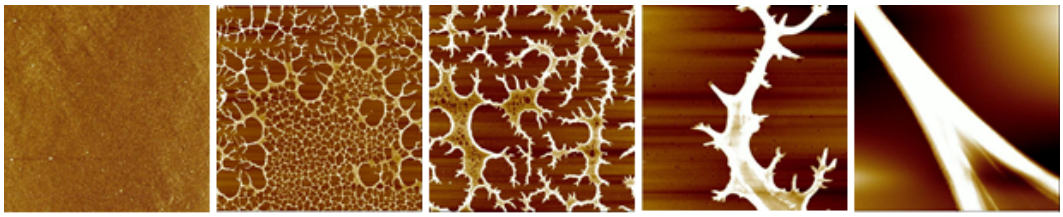

Figure 20. AFM images of PVOH on PDMS (scan size: 20 µm × 20 µm): T12 (height = 20 nm), T22 (height = 50 nm), T25 (height = 40 nm), T35 (height = 50 nm), and T46 (height = 200 nm) (from left to right).

A major research question is whether various PVOH morphologies on PDMS are formed in solution (while immersed in PVOH solution), or upon exposure to air (as soon as the substrates are taken out of the PVOH solution). Two models were hypothesized to explain the formations of different PVOH morphologies *in-situ* and *ex-situ*.

The first model is the Diffusion Limited Aggregation (DLA) model, which was proposed by Witten and Sanders in the 1980s.[56] The DLA model explains the formations of fractal features in solution. The model assumes the kinetic growth of clusters involving random walk diffusion and irreversible addition of new particles to the edges of existing, stationary features with diffusion as the rate-limiting step.[56] While the DLA model was thought to explain the formation of "fractal-like" morphologies of adsorbed PVOH seen on PDMS substrates initially, this model seems highly improbable after observing *in-situ* imaging in solution during adsorption. The reason for this is twofold: fractals were not observed in

solution and the various discrepancies in PVOH pattern formation could not be explained.

The second model is the dehydration caused "dewetting" phenomenon, which explains how fractals form upon exposure to air (*ex-situ)*. A film of hydrated PVOH on PDMS dewets to minimize energy by reducing the unfavorable solid-air and PVOH-PDMS interfaces. [48] The second model explains various morphologies formed on substrates with different molecular weights of PDMS, which will be discussed in detail in Section 3.3.

3.2 Contact angles and thickness data of adsorbed PVOH on varying molecular weights of PDMS substrates

Table 1 tabulates the contact angles and thickness values of PDMS of varying molecular weights drop-casted onto silicon wafers. As molecular weight of PDMS increased, the thickness of PDMS layer also increased. There was no obvious relationship between the thickness of PVOH layer and molecular weight of PDMS. Furthermore, the thickness of the PVOH layer on PDMS, regardless of the molecular weight of PDMS, is approximately 3.5 nm. The dynamic contact angles of PDMS substrates decreased substantially after the adsorption with PVOH.

Table 1. Contact angles and thicknesses of different molecular weights of PDMS and PVOH films on PDMS substrates.

PDMS molecular weight (Da)	**Thickness of PDMS layer (nm)**	**Dynamic contact angles of PDMS surface (Θ_A/Θ_R) (^{o})**	**Thickness of PVOH layer (nm)**	**Dynamic contact angles of PVOH on PDMS (Θ_A/Θ_R) (^{o})**
2000	1.2±0.2	103±1/99±1	3.6±0.4	79±3/13±2
9430	3.6±0.4	107±1/102±2	4.2±0.5	102±5/32±3
17250	4.4±0.4	109±1/104±1	3.5±0.9	109±1/55±6
49350	7.6±0.5	109±1/95±1	3.1±0.8	107±1/72±5
116500	11.3±0.7	113±1/98±1	2.7±1.0	112±1/93±3

Figure 21 shows the thicknesses of PDMS as a function of the molecular weights of PDMS. A positive slope indicates a positive correlation between thickness of PDMS and its molecular weight. Furthermore, the standard deviation of the thickness also increases as molecular weight of PDMS substrates increases; this means that the surface of the substrate gets rougher with increasing molecular weight of the polymer.

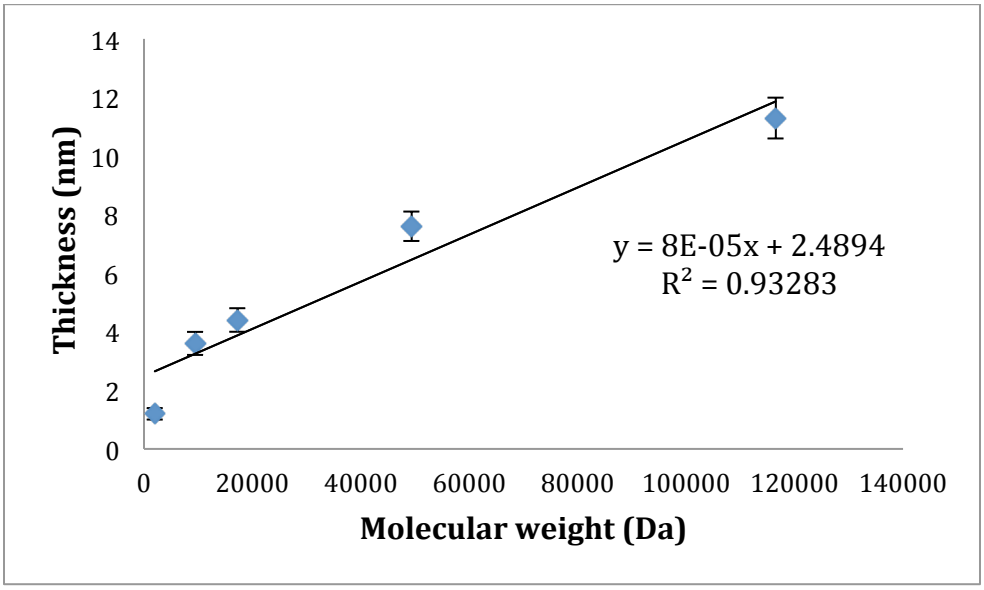

Figure 21. Graph of thickness of PDMS plotted against molecular weight of PDMS showing a near linear trend-line with a positive slope.

Figure 22 is a graph of the logarithm of thickness of PDMS layer as a function of the logarithm of molecular weight of PDMS. Logarithms of the x and y quantities were taken in order to compare the slope to the theta (θ) exponent in the following power law equation:

$$\text{Chain dimension } \alpha \text{ Molecular weight}^{\theta}.$$

Next, we can replace the proportionality constant with an equals sign and add a constant (k).

$$\text{Dimension} = k\,(\text{Molecular weight})^{\theta}$$

Taking log on both sides of the equation,

$$\log(\text{Dimension}) = \log k + \log(\text{Molecular weight})^{\theta}$$

$$\text{or, } \log(\text{Dimension}) = \theta \log(\text{Molecular weight}) + \log(k)$$

In that case, θ can be obtained by taking the slope of the graph in Figure 22. We assume the dimension to be comparable to the thickness of the PDMS chains since the PDMS chains are supposed to attach onto the silicon substrates to form a monolayer (Figure 23). The value of θ ranges from 0.5 to 0.6, where a higher θ value is indicative of a better solvent. In a good solvent, interactions between polymer segments and solvent molecules are energetically favorable, which causes polymer coils to expand.[60] In a poor solvent, polymer-polymer self-interactions are preferred, and the polymer coils will contract.[60] The slope of the graph in Figure 21 is 0.54, which means it lies between a theta solvent (θ =0.5) and a good solvent (θ =0.6). This means that there must be some solvent in the polymers.

The graph shows that there is a directly proportional relationship between the two quantities. As molecular weight of PDMS increases, the thickness of the PDMS layer on the silicon wafer also increases. This is confirmed by a slope of ~ 0.5 for the trend-line and an R^2 value very close to 1. The value of R^2 explains the data's variability from the mean. The highest value R^2 can take is 1. An R^2 value of 0.98 in this case, indicates that the data fits the model very well and there is an obvious correlation between the thickness and molecular weight of the PDMS substrate.

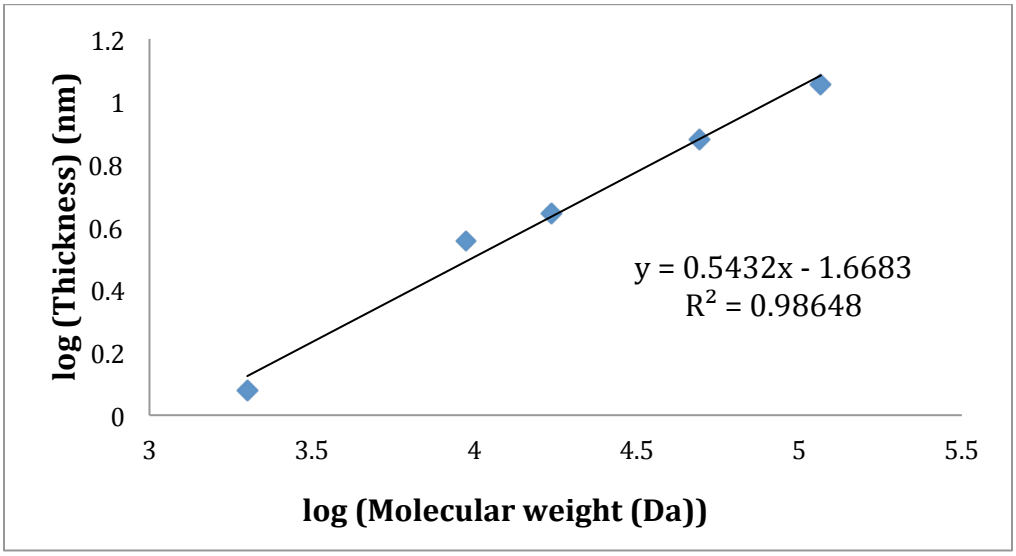

Figure 22. Graph of log (thickness of PDMS) plotted against log (molecular weight of PDMS) showing a near perfect linear trend line with a positive slope of 0.54 nm.

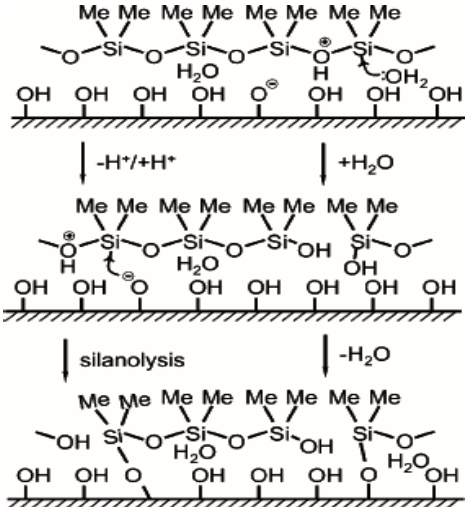

Figure 23. Covalent attachment of a PDMS linear polymer to a silicon wafer substrate.[15]

Figure 24 shows the thickness of PVOH films as a function of the molecular weights of PDMS. Although it seems like there is a negative correlation between

the two axes, the magnitude of the slope is extremely small. This leads us to conclude that the thickness of PVOH films do not depend on the molecular weight of PDMS. An interesting thing to note, however, is that standard deviation of the thickness substantially increases as the molecular weight of PDMS increases. Thus, surface heterogeneity of PVOH film increases with increasing molecular weight of PDMS.

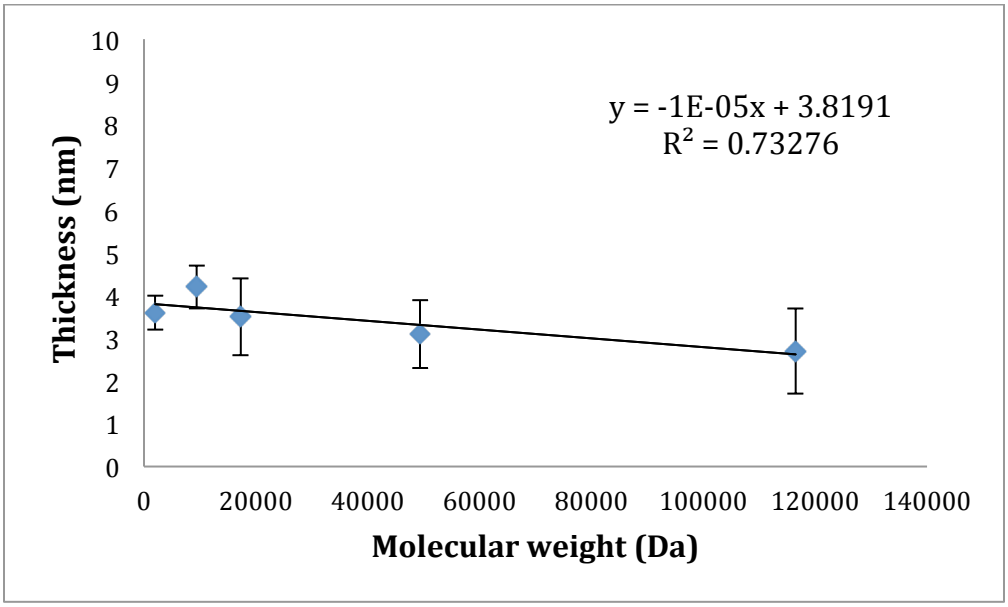

Figure 24. Graph of thickness of PVOH plotted against molecular weight of PDMS.

Figure 25 is a graph of contact angles of PDMS substrates as a function of the molecular weight of PDMS substrates. For the advancing contact angles, as the molecular weight of PDMS substrates increase, there is an overall increase in the contact angle values. The advancing contact angles are representative of PDMS hydrophobicity, which decreases as PDMS molecular weight increases. The

receding contact angle values go up from PDMS^{2000} to PDMS^{9430} and then decrease after that. The lower the receding angle, the more the extent of hydrophilization. There is not much of a difference in the hydrophilicity of the different molecular weights of PDMS substrates as they are supposed to be inherently hydrophobic, but PDMS^{2000} seems to be the most hydrophilic as indicated by its low receding contact angle value.

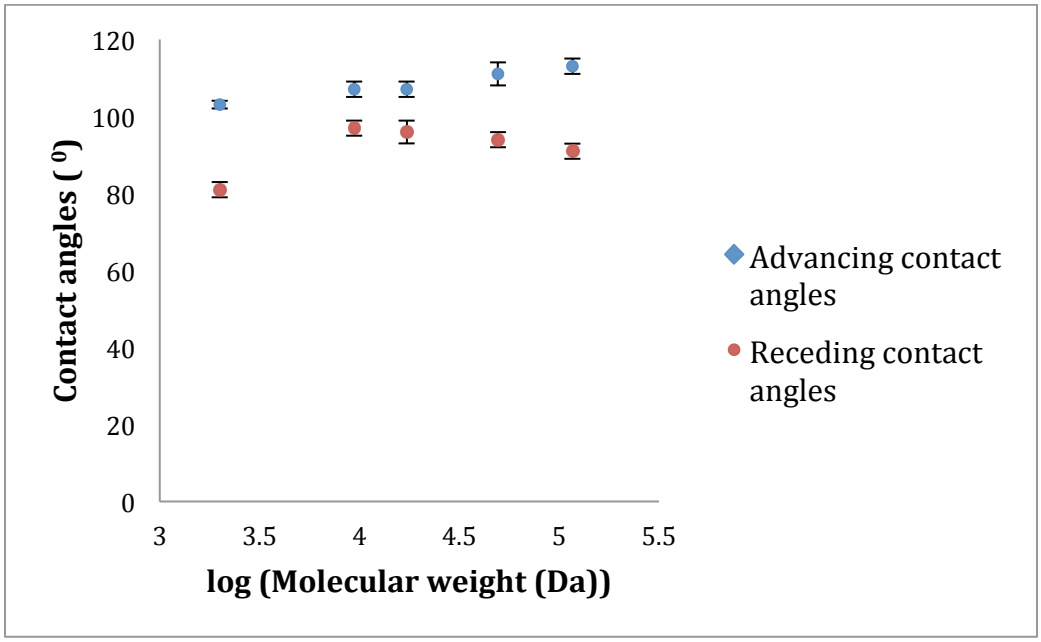

Figure 25. Graph of the dynamic contact angles of PDMS on silicon wafers plotted against the log of PDMS molecular weight.

Figure 26 is a graph of the contact angles of PVOH films as a function of the molecular weight of PDMS substrates. After the adsorption of PVOH on PDMS^{2000} substrates, the advancing and receding contact angles decreased most drastically, from 103±1/99±1^0 to 79±3/13±2^0. There is not as much reduction in

contact angles after PVOH adsorption on higher molecular weight PDMS substrates. Since the receding angles increase from $PDMS^{9430}$ to $PDMS^{116500}$, there is less coverage of PVOH with increasing PDMS molecular weights. The contact angles data corroborate with our hypothesis that various features formed upon adsorption are dependent on the molecular weight of PDMS.

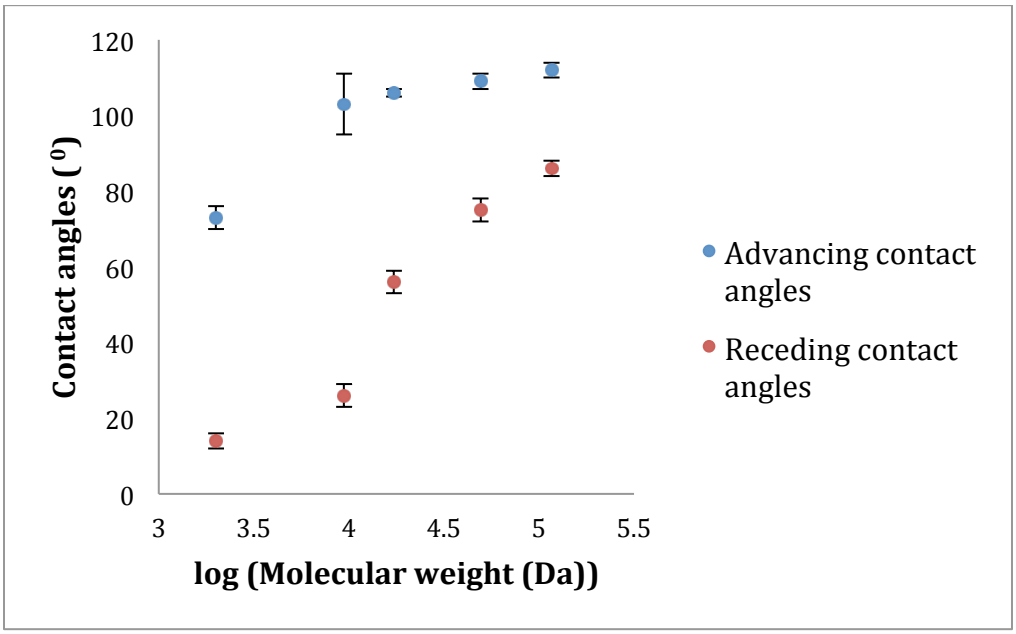

Figure 26. Graph of the dynamic contact angles of PVOH films on PDMS plotted against the log of PDMS molecular weight.

There is an overall trend of increasing advancing and receding contact angles as molecular weights of PDMS increase. The increase in advancing contact angles, as PDMS molecular weights increase from molecular weight of 2000 Da to 116,000 Da is indicative of an increase in hydrophobicity. Greater advancing contact angles indicate greater hydrophobicity. Furthermore, the increase in

receding contact angles as molecular weight of PDMS increases from 2000 Da to 116,000 Da is indicative of a decrease in surface hydrophilicity. Lower receding contact angle values mean the surface is more hydrophilic. Lower molecular weights of PDMS substrates that have lower advancing and receding contact angles have a smoother and more homogeneous coverage of PVOH films. Overall, the coverage of PVOH film on lower molecular weight PDMS substrates is much greater. Higher molecular weight PDMS substrates have high advancing and receding contact angles and are not as homogenous. The coverage of PVOH after adsorption on higher molecular weight PDMS substrates is less because the surface coverage is more heterogeneous.

A better PVOH coverage in the forms of continuous membranes and honeycomb morphologies on lower molecular weight PDMS substrates, gives rise to a significant reduction in receding angles and a somewhat reduction in advancing angles. A poor PVOH coverage in the form of fractal structures on higher molecular weight PDMS substrates, gives rise to some reduction in receding angles and minimal reduction in advancing angles. In general PVOH adsorption is more successful on lower molecular weight PDMS substrates in terms of uniformity and hydrophilicity enhancement.

3.3 Trends in PVOH morphologies upon increasing molecular weights of PDMS substrates

Varying but consistent PVOH morphologies were observed on PDMS substrates of different molecular weights. A division of morphologies will be established here. The lowest molecular weight PDMS was $PDMS^{2000}$. Figure 27 shows AFM images of the PVOH morphologies formed upon adsorbing PVOH onto a $PDMS^{2000}$ substrate.

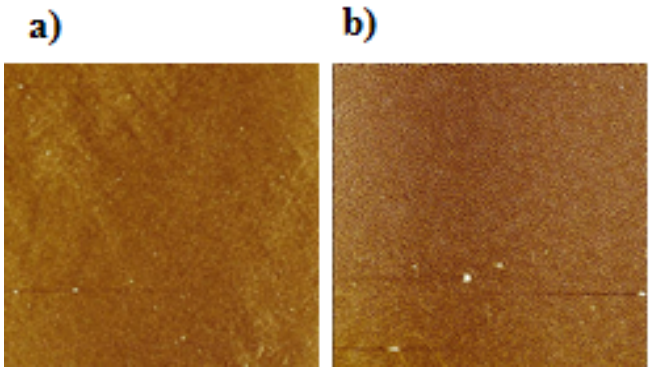

Figure 27. AFM images (scan size: 20 × 20 μm, height: 20 nm) of PVOH adsorbed on $PDMS^{2000}$: **a)** a continuous film and **b)** small honeycombs.

Two main types of morphologies formed after the adsorption of PVOH onto $PDMS^{2000}$. Continuous film morphologies and very small honeycomb structures were seen upon scanning the surfaces of these substrates. The height of these features ranged from 10-20 nm. All holes in the honeycomb morphologies were

equidistant from one another. The types of morphologies formed were the most reproducible on PDMS^{2000} substrate.

As shown in Figure 28, morphologies formed due to the adsorption of PVOH onto PDMS^{9430} were most diverse. The types of features observed ranged from continuous films to fractal features, along with transitional honeycomb and fractal morphologies. The morphologies ranged from 20 to 70 nm in height. Most features found on this substrate can be attributed to a second type of rupture mechanism of dewetting known as nucleation, which will also be discussed in the next section.

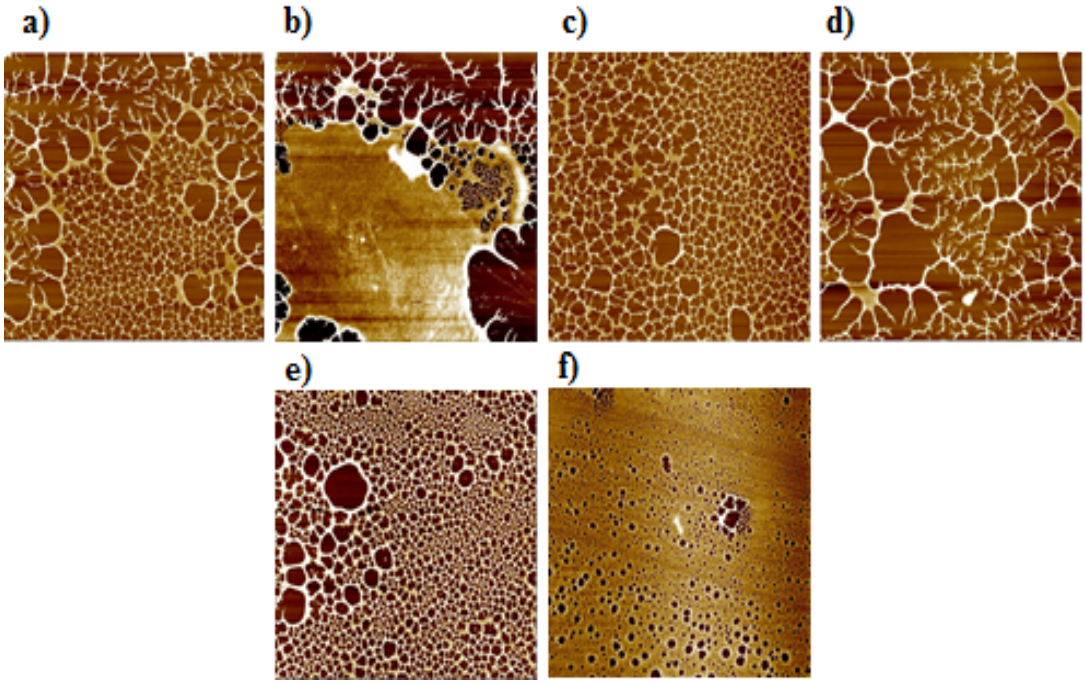

Figure 28. AFM images (scan size: 20 × 20 µm) of PVOH adsorbed on PDMS^{9430}: **a)** mixed honeycomb and fractal morphologies (height: 50 nm), **b)** mixed continuous film, honeycomb and fractal morphologies (height: 20 nm), **c)** and **d)** mixed honeycomb and fractal morphologies (height: 50 nm), **e)** big honeycombs (height: 30 nm), and **f)** small honeycombs (height: 20 nm).

Figure 29 shows the adsorption of PVOH onto PDMS^{17250}, the adsorption resulted in fractal morphologies on the substrate. No honeycomb structures were observed above this molecular weight of PDMS.

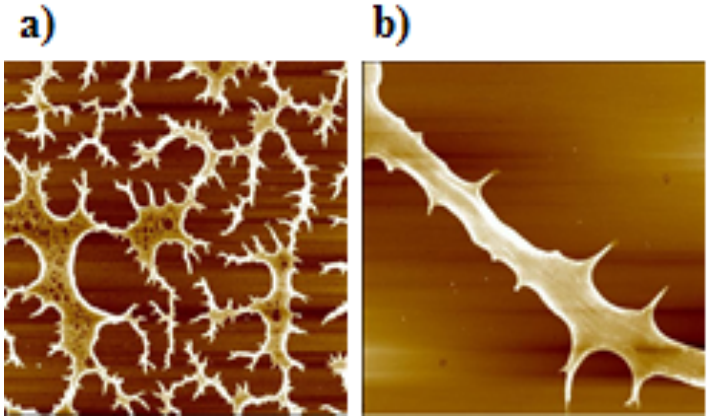

Figure 29. AFM images of PVOH adsorbed on PDMS^{17250} (scan size: 20 × 20 µm): **a)** fractal morphologies (height: 40 nm) and **b)** fractal morphologies (height: 70 nm).

Figures 30 and 31 show the adsorbed PVOH on PDMS^{49350} and PDMS^{116500} respectively. As the molecular weight of PDMS increased, the size and height of the fractal morphologies also increased. The density of fractals however decreased, making it more difficult to image a complete fractal within a 20 × 20 µm frame.

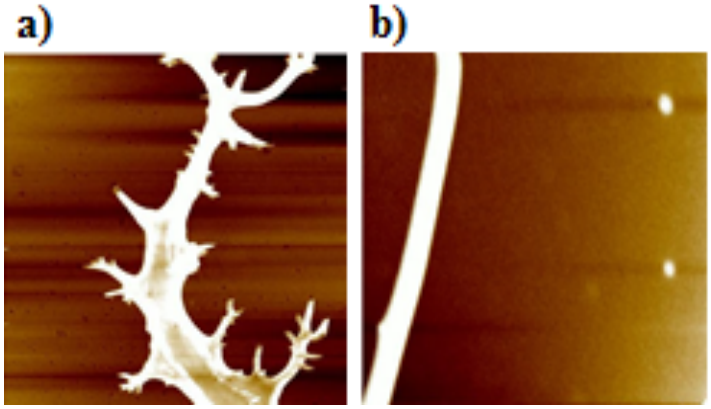

Figure 30. AFM images of PVOH adsorbed on PDMS^{49350} (height: 50 nm, scan size: 20 × 20 μm): **a)** and **b)** show different fractal morphologies.

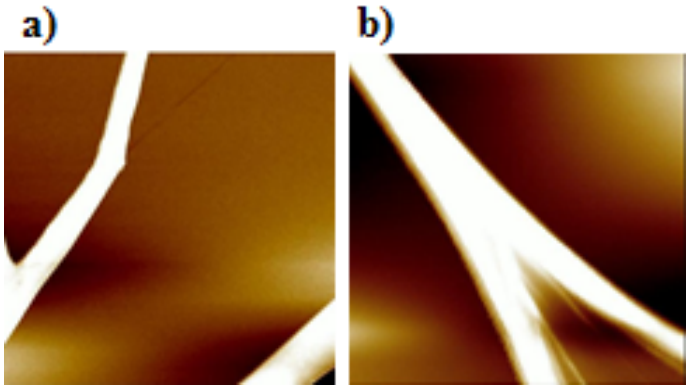

Figure 31. AFM images of PVOH adsorbed on PDMS^{116500} (scan size: 20 × 20 μm): fractal morphologies with height = 70 nm in **a)** and height = 200 nm in **b)**.

Figure 32 is a graph of the height of various features plotted against the molecular weight of PDMS. The approximate height of the features is increasing and the rate of increase is speeding up upon increasing PDMS molecular weight.

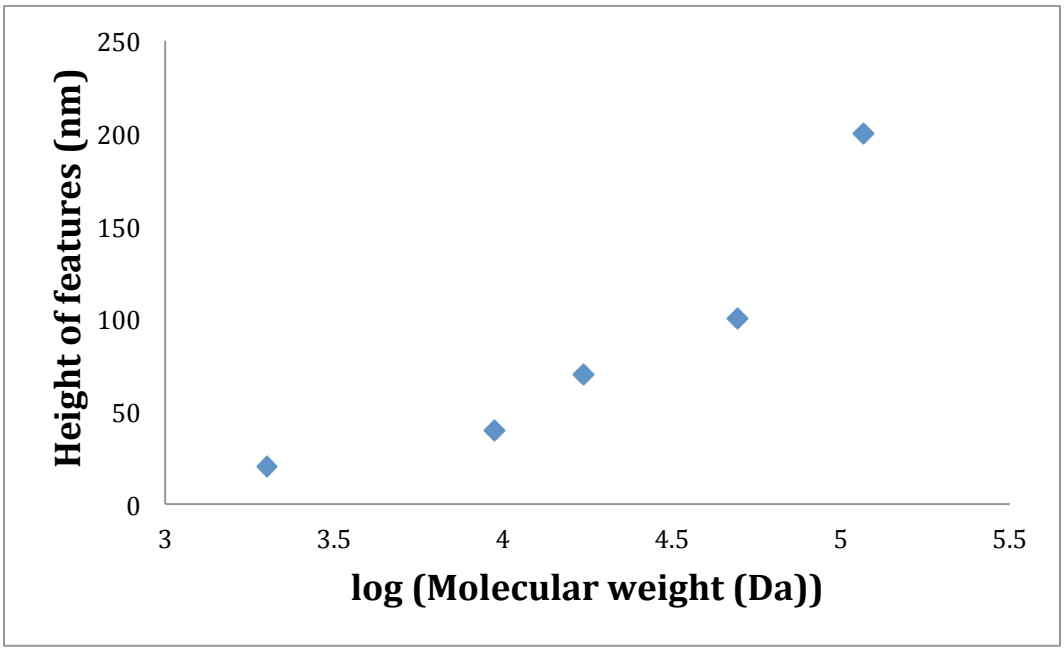

Figure 32. Graph of the feature height plotted against the log of PDMS molecular weight.

3.4 Consequences of dewetting rupture mechanisms

Two types of "dewetting" mechanisms were primarily observed: "spinodal dewetting" and "dewetting by nucleation". Earlier works of dewetting mechanisms have only been observed in cases where a polymer film is heated on a substrate and the film thicknesses are varied. In our investigation, we are seeing "dewetting-like" attributes during adsorption of uniformly thick PVOH films on different PDMS substrates, without heating.

Spinodal dewetting only occurs in unstable films. Unstable films are manifestations of thin films that change their thickness in order to minimize their

free energy.[30] Modulations of the surface of unstable films are due to fluctuations in its amplitude.[30] A result of this is a break-up of films in order to minimize the area where the liquid contacts the substrate by a dewetting process.[30] Figure 33 shows two AFM images of spinodal dewetting. A consequence and a major characteristic of spinodal dewetting is that holes that form during dewetting are equidistant from each other.

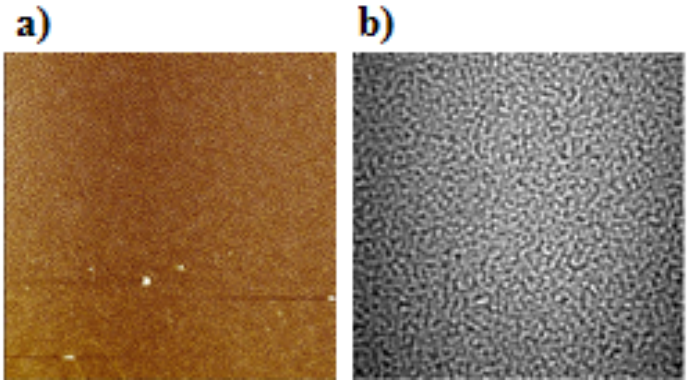

Figure 33. a) AFM image of PVOH adsorbed on PDMS[2000] due to "spinodal dewetting". **b)** AFM image of a thin poly (styrene-block-paramethyl-styrene) diblock copolymer film due to spinodal dewetting.[49]

In contrast to spinodal dewetting where holes form due to a break-up of the film, dewetting by nucleation occurs in metastable films and is initiated by first nucleating small holes.[48] Thicker films are meta-stable due to effects of gravity.[48] Consequently, holes appear at random locations. Thus, dewetting by nucleation is most often driven by heterogeneous surfaces or defects. Figure 34 shows some AFM images of dewetting by nucleation.

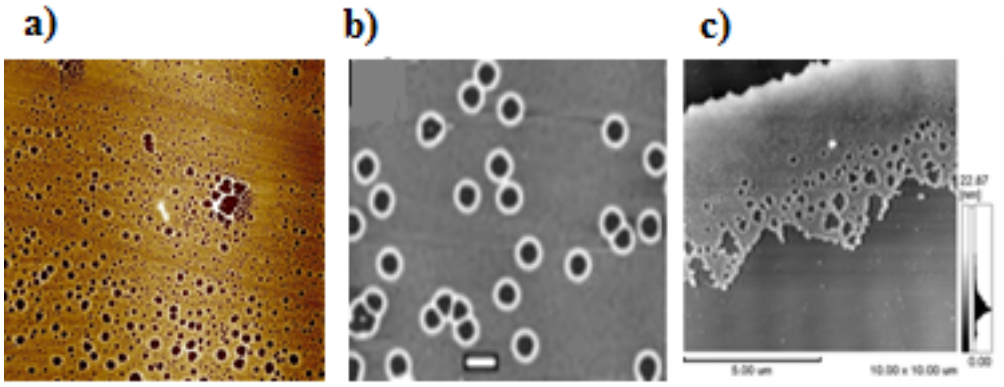

Figure 34. a) AFM image of adsorbed PVOH on PDMS[9430] because of "dewetting by nucleation". **b)** AFM image of dewetting by heterogeneous nucleation of PS (2k) films.[49] **c)** AFM image of a dewetting pattern formed by a mixture of poly (N-isopropylacrylamide) and sodium dodecyl sulfate.[50]

A type of dewetting by nucleation is known as hole coalescence. Figure 35 shows AFM images of hole coalescence. Hole coalescence can occur when film thinning is uneven and thinner regions of a film dewet ahead of the thicker regions.[50] This phenomenon occurs when a film of polymer is of a certain thickness so as to allow the polydisperse holes that are formed due to nucleation to come together in order to form a continuous film. PVOH on PDMS[9430] shows the phenomenon of a form of "hole coalescence."

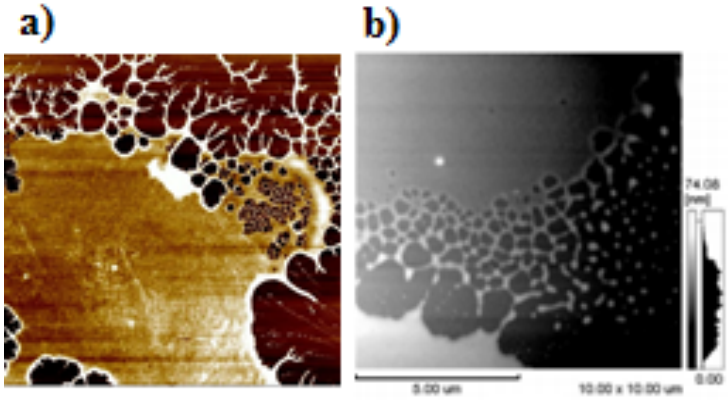

Figure 35. a) AFM image of the adsorption of PVOH on PDMS^{9430} showing hole coalescence. **b)** AFM image of dewetting pattern formed by a mixture of poly (N-isopropylacrylamide) and sodium dodecyl sulfate.[50]

In Figure 36, section analysis of AFM images depicting adsorbed PVOH on PDMS^{9430} is done. The analysis reveals that the thickness of the PVOH film on PDMS^{9430} is roughly about 7-8 nm. The increase in continuous film thickness can be attributed to the coalescence of holes and accumulation of more PVOH polymer in surrounding areas.

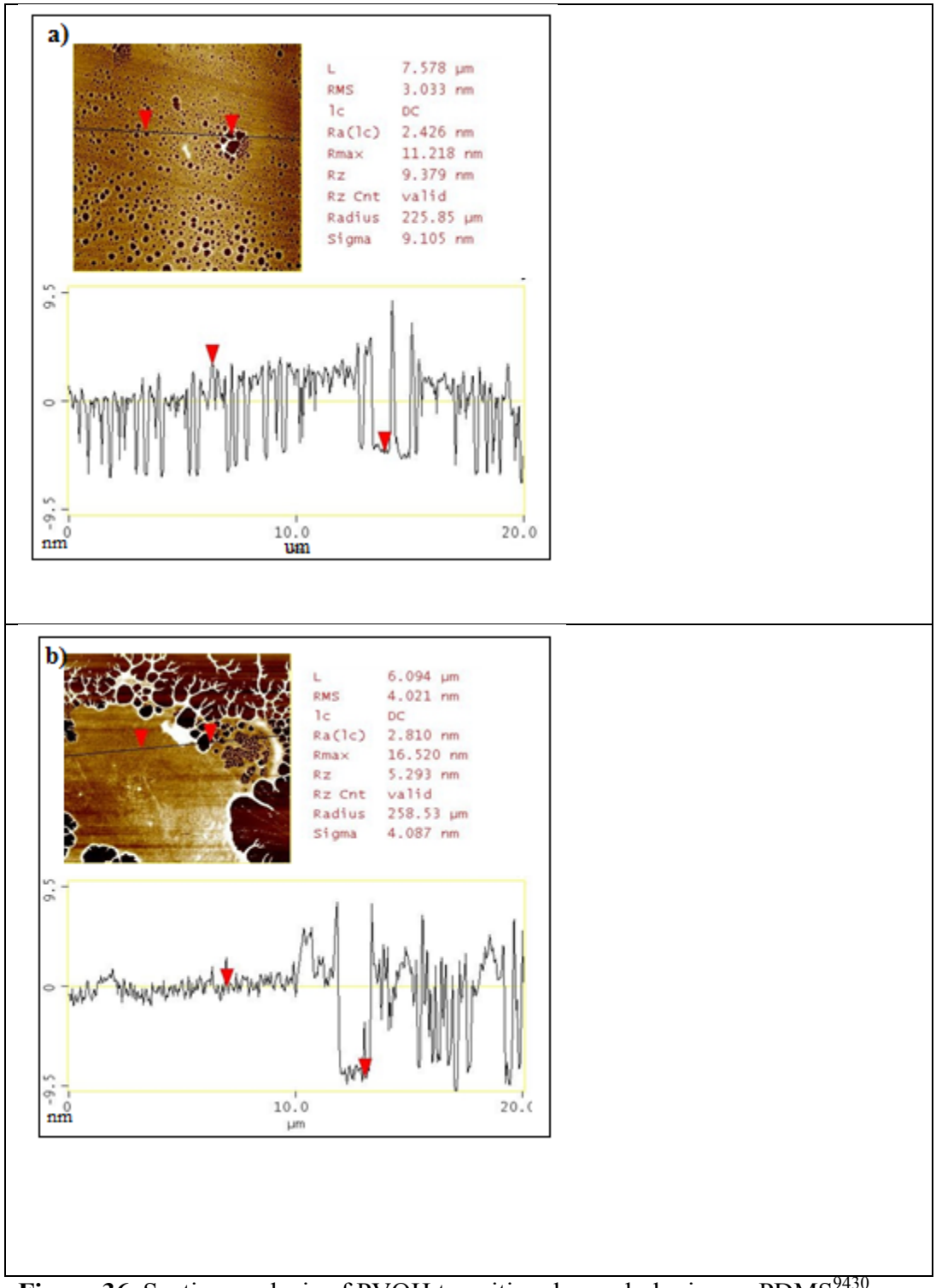

Figure 36. Section analysis of PVOH transitional morphologies on PDMS[9430] showing **a)** honeycomb structures and **b)** transitional morphologies.

Similarly, Figure 37 shows the section analysis of a PVOH film that has undergone “spinodal dewetting”. The analysis reveals that the heights of the holes are ~3 nm. The PVOH layer formed upon adsorption is also roughly 3 nm thick. This means that the film is discontinuous at areas where there are holes. The holes form all the way through the layer of PVOH.

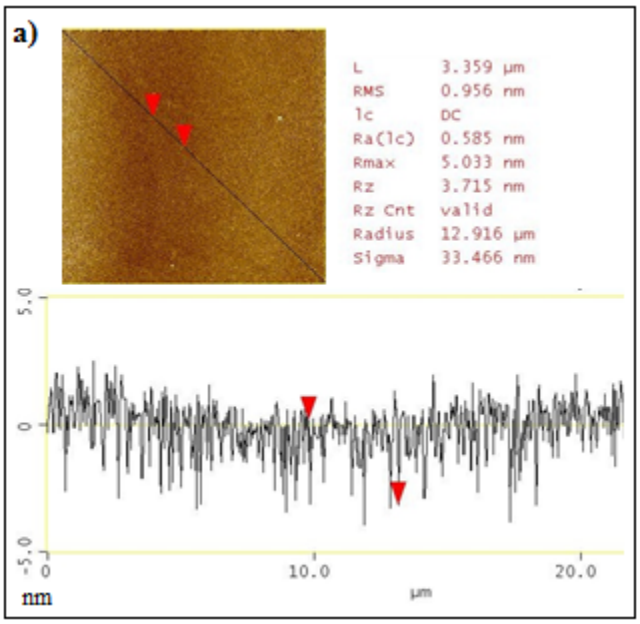

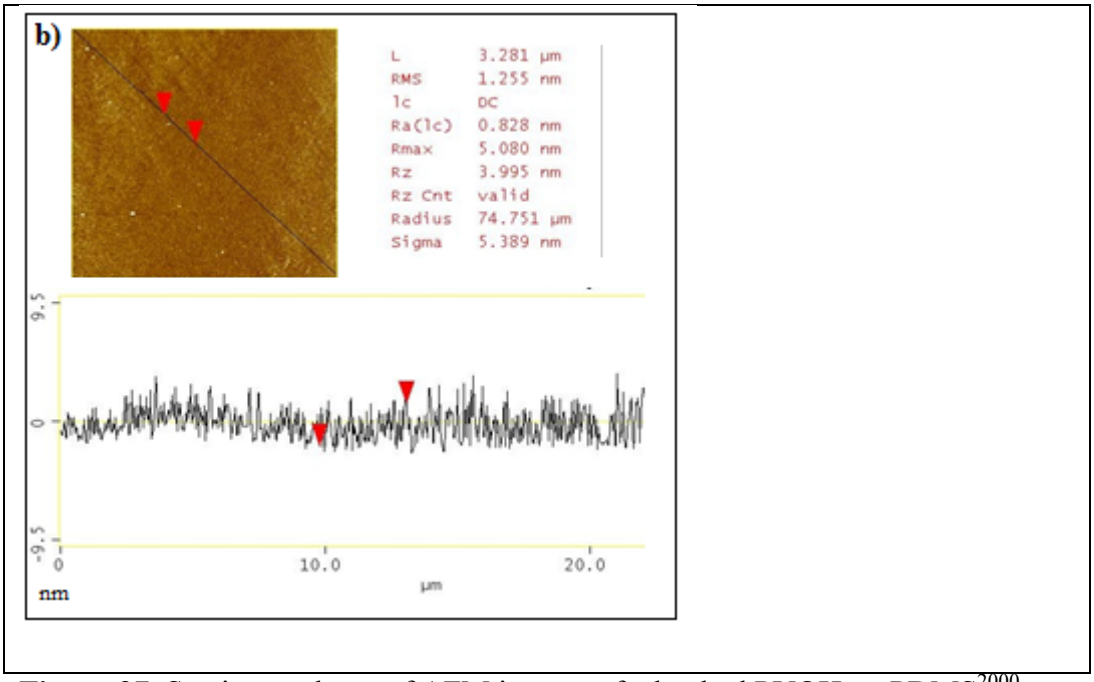

Figure 37. Section analyses of AFM images of adsorbed PVOH on PDMS^{2000} substrates showing continuous films of heights a) 10 nm and b) 20 nm.

The implications of the different "dewetting" methods can be seen in the different morphologies formed after PVOH adsorption, where continuous membranes are a consequence of the "spinodal dewetting" of unstable films. Furthermore, honeycombs structures can be attributed to "heterogeneous dewetting by nucleation" of metastable films. While fractal morphologies have never been observed in a dewetting scenario, it could be that fractals are an extreme case of "dewetting by nucleation". This is further supported by the fact that the adsorbed PVOH on PDMS^{9430} has various transitional morphologies where transitions between fractals and honeycombs take place. Since, it is difficult to distinguish metastable and unstable mechanisms experimentally, both nucleation and spinodal dewetting can lead to dewetting in unstable films.[49] This

can then explain the formations of both continuous films and honeycomb structures due to "spinodal dewetting" and "dewetting by nucleation" after the adsorption of PVOH on $PDMS^{2000}$ substrates.

It must be made clear that in the dewetting studies done in the past, the formation of distinct dewetting types were largely attributed to the differences in thicknesses of the substrates. Figure 11 in section 1.6 succinctly illustrates the dependence of a substrates' thickness to its dewetting behavior. However, in this case, we have PVOH of similar thicknesses on different PDMS substrates. Even so, we are seeing varying "dewetting-like" morphologies. Due to this reason, we can confirm that the mechanism of formation of distinct PVOH morphologies is not quite like dewetting. Even though PVOH thickness is the same across the five different molecular weights of PDMS, the PVOH morphologies follow one of two dewetting types depending on the molecular weights of the underlying PDMS substrates. A hypothesis is presented below for the differences in PVOH morphologies seen and their similarities with dewetting behavior.

Hypothesis 1. PVOH morphologies formed on different PDMS substrates are due to differences in density of defects in lower and higher molecular weights of underlying PDMS substrates. Lower molecular weight substrates have fewer number of defects as indicated by their root mean square roughness values, and form uniform and small-sized holes. These correspond to the morphologies formed via "spinodal dewetting". Higher molecular weight PDMS substrates have

more surface defects and form non-uniform bigger sized holes resembling "dewetting by nucleation". Coverage of a smooth and uniform PVOH layer becomes more difficult due to the increasing roughness of PDMS substrates as PDMS molecular increases.

3.5 *In-situ* imaging of adsorption and desorption

Time-lapse imaging using *in-situ* optical microscopy was done to determine whether PVOH morphologies formed on PDMS in solution or upon exposure to air. A camera attached to a microscope captured images during the adsorption of PVOH on $PDMS^{49350}$ and $PDMS^{2000}$ substrates. Figures 38 and 39 show the 24 images taken during a 24-hour adsorption period of on $PDMS^{2000}$ and $PDMS^{49350}$, respectively. $PDMS^{2000}$ was used as a control, since fractal features do not form on this substrate. All the images are identical with no additional features observed during the 24 h adsorption period in solution, implying that PVOH fractals do not form *in-situ*. Upon taking the samples out of the PVOH solution, the instantaneous formation of fractals were observed with the naked eyes. This indicates that fractals are formed upon exposure to air.

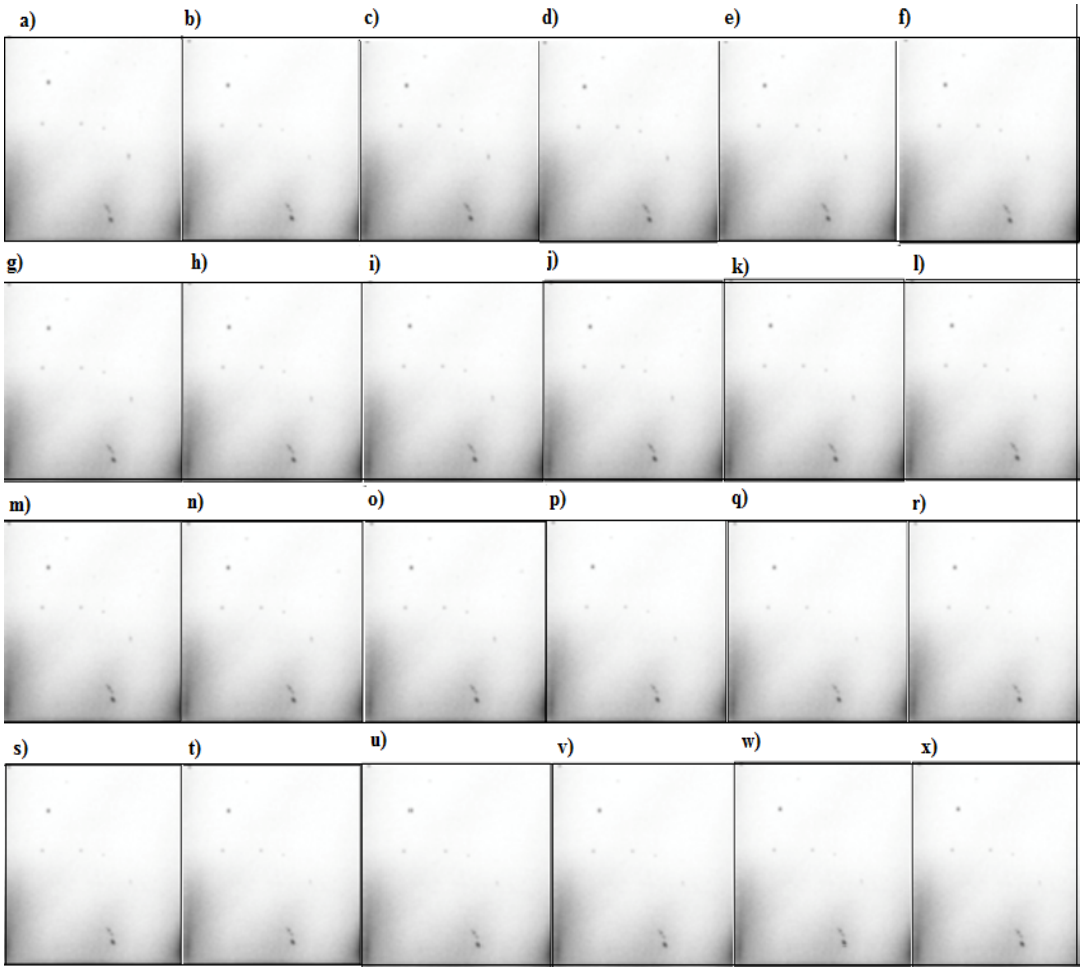

Figure 38. a-x) Optical microscope time-lapse images of *in-situ* PVOH adsorption on PDMS^{2000} taken over a 24-h period with 1-h time intervals. The spots are due to dust particles on the camera lens.

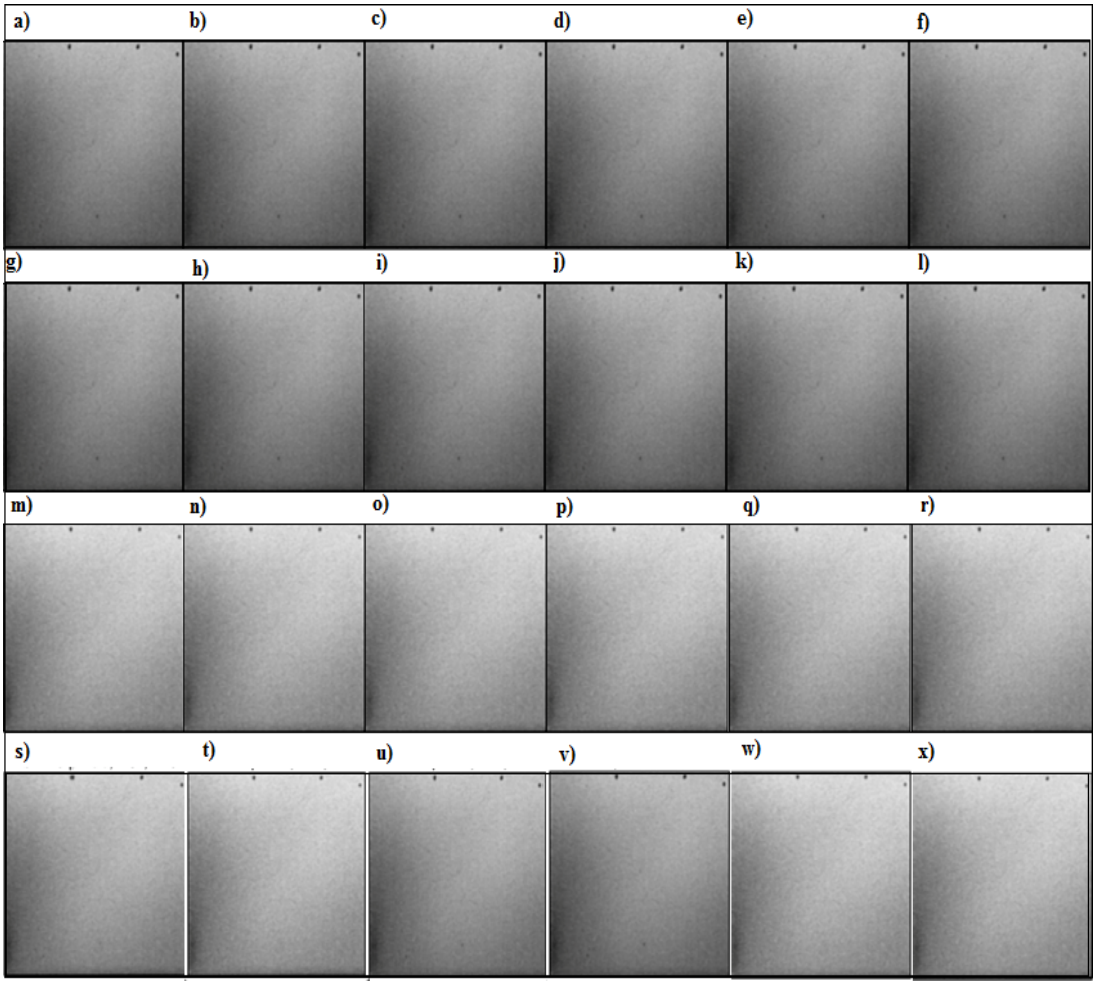

Figure 39. a-x) Optical microscope time-lapse images of *in-situ* PVOH adsorption on PDMS^{17250} taken over a 24-h period with 1-h time intervals.

Furthermore, desorption of PVOH on PDMS^{49350} substrates was also carried out using *in-situ* microscopy. Time-lapse images were taken during a 24 h desorption of PVOH on PDMS^{49350} substrates. In determining whether PVOH desorbed in water, the samples were immersed in water for a 24 h period and a series of images were taken over a 24 h period as shown in Figure 40. The fractal-

like features remain after 24 h of soaking in water. *In-situ* desorption imaging suggests that adsorbed PVOH films, upon drying, do not desorb in water.

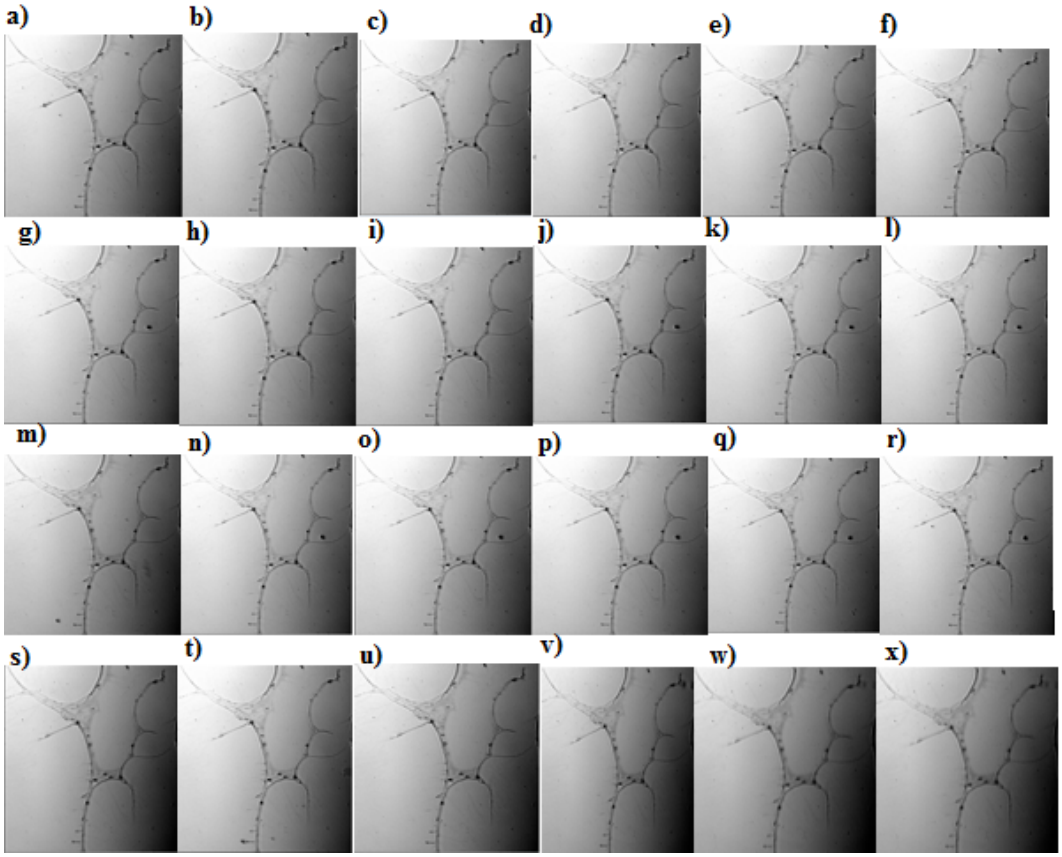

Figure 40. a-x) Optical microscope time-lapse images of desorption of PVOH on PDMS^{17250} taken over a 24-h period with 1-h time intervals.

3.6 Solubility tests and desorption of PVOH on $PDMS^{2000}$ and $PDMS^{9430}$

Three solubility tests were carried out to determine the stability of adsorbed PVOH on PDMS. AFM was used to capture changes in morphologies on $PDMS^{2000}$ substrates and optical microscopy was used to characterize the fractal features formed on $PDMS^{49350}$. PVOH morphologies on $PDMS^{2000}$ substrates remained more or less the same in all three solubility tests as shown in Figure 41. There is slight loss in PVOH thickness after solubility test 3, but the difference is within the standard deviation of the averaged values. The difference in PVOH solubility was more apparent on $PDMS^{49350}$, which is depicted in Figure 42.

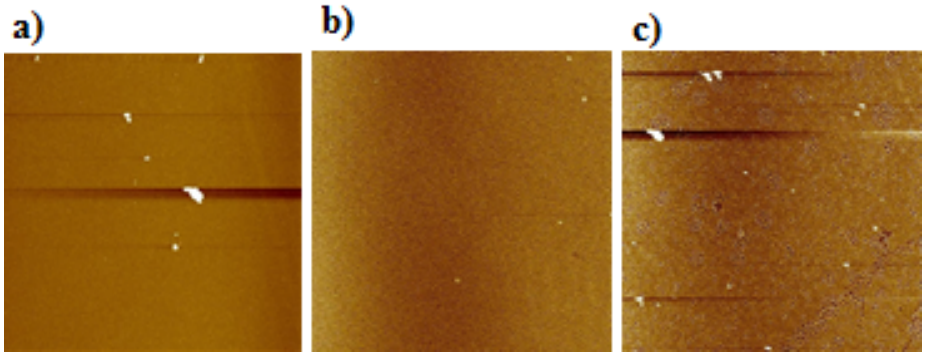

Figure 41. AFM images of PVOH on $PDMS^{2000}$ (scan size: 20 µm × 20 µm; height: 10 nm) **a)** after solubility test 1 (thickness: 2.8±0.1 nm), **b)** solubility test 2 (thickness: 2.8±0.4 nm), and solubility test 3 (thickness: 2.6±0.1 nm,) (from left to right).

It can be seen from Figure 41 that fractal morphologies were observed after solubility tests 2 and 3 while continuous-film morphology was captured after solubility test 1. This difference in morphology could be attributed to the role of water as a plasticizer in film formation and stabilization.[59]

Plasticizers are small molecules that are mobile and move easily through polymer matrices. They lower the energy requirements for large-scale mobility of polymer chains. While doing so, plasticizers disrupt the crystallinity of a polymer and make it softer.[59] Overall they increase the "free volume" of a polymer.[59]

In solubility test 1, the wafers were never taken out of water; they were simply left inside the Schlenk tube for 24 h after the 7× dilution. It could be that water's role as a plasticizer was most efficient in test 1 due to the lack of air exposure leading to a decrease in PVOH crystallinity. In solubility test 2, there was a brief exposure to air after which the wafers were placed again in water. This short exposure to air might result in some dehydration of the PVOH film and a lesser effect of water as a plasticizer. This would also give rise to a more crystalline PVOH film.

Finally, solubility test 3 was the test with overnight drying of samples in a desiccator before placing them back in water. The long period of drying could lead to complete PVOH dehydration and crystallization. It must also be noted that the solution used for solubility test 1 contained a mixture of water and residual PVOH solution, differed from that used in solubility tests 2 and 3, which only contained water. This discrepancy might have somehow affected "dewetting" and crystallization of the polymer films. But the exact reasons remain elusive. Results from the solubility tests will remain ambiguous until crystallization of PVOH films is characterized in the near future.

In terms of PVOH film thickness, solubility test 3 differed from solubility tests 1 and 2. The discrepancies in thicknesses, again, had to do with the duration of drying. Solubility tests 1 and 2 were placed in water without drying or with a few seconds of drying. Due to this reason, there was a greater possibility for solvent (water) annealing in tests 1 and 2, which made the films more stable and thicker.

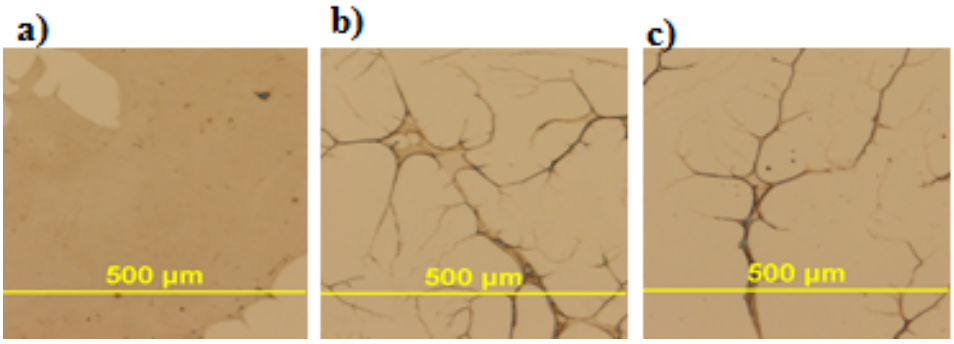

Figure 42. Optical microscope images of PVOH on PDMS[9430] **a)** solubility test 1 (thickness: 2.6±1.1 nm), **b)** solubility test 2 (thickness: 2.8±0.5 nm), and solubility test 3 (thickness: 1.8±0.8 nm).

Table 2 answers one of the major research questions of this research: Is the PVOH film soluble in water?

Table 2. Thickness of PVOH films on $PDMS^{49350}$ and $PDMS^{2000}$ before and after desorption in water.

	Thickness before (nm)	**Thickness after (nm)**
$PDMS^{49350}$	2.6±0.6	2.4±0.5
$PDMS^{2000}$	3.0±0.2	2.7±0.4

PVOH film thickness on $PDMS^{49350}$ and $PDMS^{2000}$ substrates decreased by 0.2 nm and 0.3 nm, respectively, after being submerged in water for 24 h. Desorption measurements in Table 2 were obtained in the spring semester of 2015, and differ in thickness values from the desorption results done over the summer of 2014. The most recent desorption results indicate that there is minimal desorption of PVOH upon submerging them back in water, which means that PVOH film is largely insoluble in water. In terms of morphology, there was negligible change on $PDMS^{2000}$ before and after desorption. In the case of $PDMS^{49350}$, the morphology changed from wide to thin fractals as shown in Figure 42. If consistent with the proposed hypothesis, there is also a decrease in crystallinity from image a to b. Although the adsorbed PVOH does not desorb in water after drying, they might continue to crystallize, or become ordered by contracting to form sharper and higher features as shown in Figure 43.

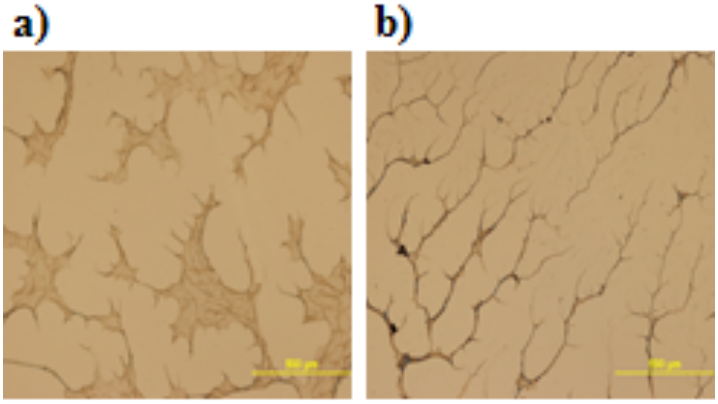

Figure 43. Optical microscope images of PVOH on PDMS^{49350} substrates **a)** before and **b)** after soaking in water for 24 h.

3.7 Adsorption kinetics

PVOH adsorptions for 24 h and 15 min are shown in Figure 44, which confirm the rapid nature of adsorption. The 24 h adsorption had a PVOH thickness of 3.5±0.9 nm, whereas the 15 min adsorption had a PVOH thickness of 2.2±0.2 nm. Within just 15 min, almost 70% of the PVOH film had adsorbed onto the substrate. However, the surfaces after the 15 min adsorption were rougher than the 24 h adsorption, with conspicuous holes. This implies that the 15 min adsorption was incomplete.

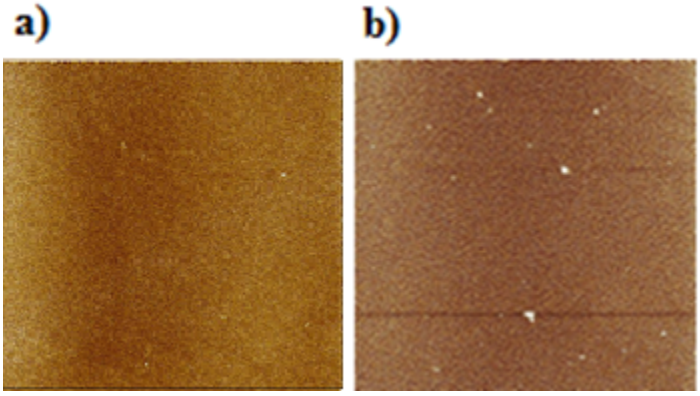

Figure 44. AFM images of PDMS^{2000} (scan size: 20 μm × 20 μm; height: 10 nm): **a)** after 24 h adsorption (thickness: 3.5±0.9 nm) and **b)** after 15 min adsorption (thickness: 2.2±0.2 nm).

3.8 Re-adsorption of PVOH

A second 24-hour PVOH adsorption was done on PDMS^{2000} that was already adsorbed with PVOH. The objective of re-adsorption was to find out whether the second layer of PVOH adsorbed on top of the first layer of PVOH or on bare PDMS. This would give us some idea of whether the strength of interaction between PVOH chains is stronger than the interactions between PDMS and PVOH chains. Table 3 tabulates the results obtained after wafers were adsorbed with PVOH once and twice.

Table 3. Thickness and rms values of adsorption and re-adsorption of PVOH onto $PDMS^{2000}$.

	Thickness of PVOH (nm)	**AFM rms (nm)**
Adsorbed layer of PVOH	3.6±0.4	0.9
Re-adsorbed layer of PVOH	2.2±0.3	0.5

From Table 3, we can deduce that the re-adsorbed layer is about 61% of the adsorbed layer. On $PDMS^{2000}$, because the first adsorbed PVOH layer is continuous, the re-adsorbed layer has to be on top of the initial layer, likely driven by hydrogen bonding. Conducting this experiment on other substrates where the initial PVOH film is discontinuous could reveal more about the re-adsorption behavior of PVOH. Lastly, measurement of crystallinity could also be vital in this investigation to make any further assertions.

IV. CONCLUSIONS AND FUTURE DIRECTION

4.1 Conclusions

The thickness of the PDMS substrate drop-casted onto the silicon wafer increased as a function of increasing PDMS molecular weights. The thickness of the layer of PVOH film adsorbed was independent of the molecular weight of the PDMS substrate. A better PVOH coverage in the form of continuous membranes and honeycomb morphologies on lower molecular weight PDMS substrates gave rise to a significant reduction in receding angles and a somewhat reduction in advancing angles. A poor PVOH coverage in the form of fractal structures on higher molecular weight PDMS substrates gave rise to some reduction in receding angles and a minimal reduction in advancing angles. In general, PVOH adsorption was more successful on lower molecular weight PDMS substrates.

As molecular weight of PDMS increased, the morphology of the PVOH films formed upon adsorption changed from continuous films to honeycomb structures to fractal features. Different morphologies were most likely forming upon the substrates' exposure to air (*ex-situ*). On lower molecular weight PDMS, the adsorbed PVOH continuous films were most likely consequences of a type of "spinodal dewetting".

With increasing PDMS molecular weight, there was also an increase in the PDMS chain flexibility and the number and/or extent of defect sites on the substrate, which gave rise to a type of "dewetting by nucleation", thereby

explaining the honeycomb morphologies, transitional structures, and fractal features that were observed. Unlike previous studies of dewetting where types of dewetting were dependent on the thickness of the layer that dewets, dewetting of PVOH is not dependent on the thickness of the PVOH films. In this investigation, the thicknesses of PVOH films are more or less the same across all PDMS molecular weights. Due to this reason, morphologies of substrates that undergo "spinodal dewetting" and "dewetting by nucleation" are similar to the PVOH morphologies seen, but their mechanisms of formation are different. The instability of the adsorbed PVOH thin films was most likely caused by surface chemical and/or physical "defects": lower molecular weight PDMS resulted in incomplete surface coverage exposing surface silanol groups while larger molecular weight PDMS covered the silicon wafer substrates completely with significant roughness. The instability of the adsorbed films could also be dependent on the thickness of the underlying PDMS film.

The solubility tests were able to elucidate water's role as a plasticizer and also provide an inference about reasons a plasticizer's efficiency could be compromised. It also gave insights on the cause of thicker PVOH films, which could be attributed to an increase in mobility as a result of better annealing. Finally, we were able to answer one of the vital questions of our investigation and deduce that PVOH films do not desorb in water.

Re-adsorption of $PDMS^{2000}$ confirmed that the re-adsorbed layer was on top of the initial layer, likely driven by hydrogen bonding. The roughness of the wafer

also decreased upon re-adsorption. The effect of re-adsorption on other substrates, as well as the investigation of its driving forces is yet to be done.

4.2 Future directions

A "dewetting-like" phenomenon occurs when PVOH is adsorbed onto PDMS substrates giving rise to different morphologies of PVOH on PDMS substrates of varying molecular weights. We are yet to establish the general rules for understanding the rupture mechanisms involved in this "dewetting" process. It is much harder to determine what is happening in the case of higher molecular weight PDMS substrates. More specifically, what particular changes the fractal height, width, and size are undergoing as PDMS molecular weight increases are still under scrutiny. Perhaps after understanding this, we can establish ways to actively minimize "dewetting".

Furthermore, there is a need to measure the crystallinity of the PVOH films in order to ascertain the role played by water as a plasticizer. The crystallinity data can also be compared with other adsorption kinetics tests in order to probe deeper into the factors accounting for film morphologies and thicknesses. Without measuring the crystallinity of the PVOH films, we cannot corroborate the implications caused by the solubility tests.

Re-adsorption was an interesting toolkit used to probe deeper into our understanding of fractal formations. Using the $PDMS^{2000}$ substrate, it was established that the second layer of PVOH adsorbs onto the initial PVOH layer.

Investigating effects of re-adsorption on other PDMS substrates will allow us to figure out the driving forces involved in this process.

Finally, varying the degree of hydrolysis of PVOH, and seeing its effects on PVOH film morphology on the PDMS substrates may reveal some more things about the “dewetting-like” process.

REFERENCES

1. McDonald J. C.; Whitesides G. M. Poly(dimethylsiloxane) as a Material for Fabricating Microfluidic Devices Acc. Chem. Res. **2002**, *35*, 491-499.
2. Almutairi, Z.; Ren, C. L.; Simon, L. Evaluation of polydimethylsiloxane (PDMS) surface modification approaches for microfluidic applications. Colloids Surf. Physicochem. Eng. Aspects **2012**, *415*, 406-412.
3. Prakash A. R.; Adamia S.; Sieben V.; Pilarski P.; Pilarski L. M.; Backhouse C. J., Small volume PCR in PDMS biochips with integrated fluid control and vapor barrier, Sensors and Actuators B **2006**, *113*, 398-409.
4. Moorcroft, M. J; Wouter, R. A; Meuleman; Latham, S. J; Nicholls T. J; Egeland R. D; Southern, E. M. In Situ oligonucleotide synthesis on poly(dimethylsiloxane): a flexible substrate for microarray fabrication, Nucleic Acids Research **2005,** *33,* 1-4.
5. C. S. Effenhauser; G. J. M. Bruin; A. Paulus; M. Ehrat, Integrated Capillary Electrophoresis on Flexible Silicone Microdevices: Analysis of DNA Restriction Fragments and Detection of Single DNA Molecules on Microchips. Anal. Chem **1997**, *69,* 3451-3457.
6. Christopher G. F.; Anna S. L. Microfluidic methods for generating continuous droplet streams J. Phys. D: Appl. Phys. **2007**, *40*, R319-R32.
7. Garstecki P.; Gañán-Calvo A. M.; Whitesides G. M. Formation of bubbles and droplets in microfluidic systems Pol. Acad. Sci.: Tech. Sci. **2005**, *53*, 361.
8. Kakuta M.; Bessoth F. G.; and Manz A. Microfabricated devices for fluid mixing and their application for chemical synthesis Chem. Rec. **2001**, *1*,395.
9. Ibarlucea B.; Fernández-Sánchez C.; Demming S.; Büttgenbach S.; Llobera A. Biofunctionalization of PDMS-based microfluidic systems. IMB-CNM **2011**, 1-2.
10. Slentz, B.E.; Penner, N.A.; Lugowska, E.; Regnier, F. Nanoliter capillary electrochromatography columns based on collocated monolithic support structures molded in poly(dimethyl siloxane). Electrophoresis, **2001**, *22*, 3736-3743.
11. Bodas D.; Khan-Malek C. Hydrophilization and hydrophobic recovery of PDMS by oxygen plasma and chemical treatment – An SEM investigation. Sens. Actuators B. **2001**, *123*, 368-373.
12. Berdichevsky Y.; Khandurina J.; Guttman A.; Lo Y.H. UV/Ozone modification of Poly(dimethylsiloxane) microfluidics channels. Sens. Actuators B., **2004**, *97*, 402-408.

13. Sui G. et al. Solution-phase surface modification in intact poly(dimethylsiloxane) microfluidic channels. *Anal. Chem.* **2006**, *78,* 5543-5551.
14. Kozlov, M.; McCarthy, T. J. Adsorption of Poly(vinyl alcohol) from Water to a Hydrophobic Surface: Effects of Molecular Weight, Degree of Hydrolysis, Salt, and Temperature. Langmuir **2004**, *20,* 9170-9176.
15. Krumpfer, J. W.; McCarthy, T. J. Rediscovering Silicones: 'Unreactive' Silicones React with Inorganic Surfaces. Langmuir **2011**, *27,* 11514-11519.
16. Peiwen Zheng, "Preparation, Characterization, Surface Modification And Applications Of Siloxane Polymers." Ph.D. Dissertation, University of Massachusetts Amherst, MA, **2012**.
17. Johana Kuncová-Kallio "PDMS and its Suitability for Analytical Microfluidic Devices" Student Member IEEE, **2006**.
18. Wanxin Wang, "Preparation and surface PEGylation of crosslinked Polydimethylsiloxane substrates with tunable moduli." Undergraduate Thesis, Mount Holyoke College South Hadley, MA, **2013**.
19. Polyvinyl Acetate to Polyvinyl Alcohol." Materialsworld.utep.edu. Dr. Michael Eastman, n.d. Web. 24 Feb. **2014**.
20. Poly(vinylalcohol) (PVA)." Encyclopaedia Britannica. Encyclopaedia Britannica Online Academic Edition. Encyclopædia Britannica Inc., **2014**. Web. 23 Feb. 2014.
21. Yu, L.; Li, C. M.; Zhou, Q.; Luong, J. H. T. Poly(vinyl alcohol) Functionalized Poly(dimethylsiloxane) Solid Surface for Immunoassay, Bioconjugate Chem **2007**, *18*, 281-284.
22. Makadia, H.K.; Siegel, S.J. Poly Lactic-co-Glycolic Acid (PLGA) as Biodegradable Controlled Drug Delivery Carrier. Polymers **2011**, *3*, 1377-1397.
23. Hassan, C. M.; Peppas, N. A. In Structure and applications of poly (vinyl alcohol) hydrogels produced by conventional crosslinking or by freezing/thawing methods; Biopolymers• PVA Hydrogels, Anionic Polymerisation Nanocomposites. Springer **2000**, *1*, 37-65.
24. http://en.wikipedia.org/wiki/Polyvinyl_alcohol. (Accessed March 2014).
25. http://www.polymerprocessing.com/polymers/PVOH.html (Accessed April 2014).
26. Hong L.; Dafu W.;Huining X.; Anna Z.; Fuzeng H. Synthesis and characterization of a thermal sensitive polyelectrolyte based on poly(vinyl alcohol) and its thermal sensitive properties. Acta Polymerica Sinica **2007***, 12*, 1161-1167.

27. Wong, I.; Ho, C. M. Surface Molecular Property Modifications for Poly (dimethylsiloxane) (PDMS) Based Microfluidic Devices. Microfluid. Nanofluid **2009**, *7*, 291-306.
28. Kozlov, M.; Quarmyne, M.; Chen, W.; McCarthy, T. J. Adsorption of Poly(vinyl alcohol) to Hydrophobic Substrates: A General Approach for Hydrophilizing and Chemically Activating Surfaces. Macromolecules **2003**, *36*, 6054-6059.
29. "Langmuir Equation." Wikipedia. Wikimedia Foundation, **2014**. Web. (Accessed July 2014).
30. Gentili, D.; Foschi G.; Valle F.;Cavallini M.; Biscarni F. Applications of dewetting in micro and nanotechnology. Chem. Soc. Rev **2012**, *41*, 4430-4443.
31. P. G. de Gennes, Wetting: statics and dynamics. Rev. Mod. Phys **1987**, *57*, 827–863.
32. Reiter G. Unstable Thin Polymer Films: Rupture and Dewetting Processes. Langmuir **1993**, *9,* 1344-1351.
33. A. Sharma, Relationship of thin film stability and morphology to macroscopic parameters of wetting in the apolar and polar systems. Langmuir **1993**, *9*, 861–869.
34. P.-G. de Gennes; F. Brochard-Wyart; D. Quere, Capillarity and Wetting Phenomena: Drops, Bubbles, Pearls, and Waves. Springer, **2004**.
35. Telford A.; Meagher L.; Glattauer V.; Gengenbach T. R.; Easton C.; Neto C. Micropatterning of Polymer Brushes: Grafting from Dewetting Polymer Films for Biological Applications. Biomacromolecules **2012**, *13*, 2989−2996.
36. Advincula, R. C.; Brittain, W. J.; Caster, K. C.; Ruhe, J. Polymer Brushes: Synthesis, Characterisation, Applications; Wiley-VCH: Weinheim. Germany, **2004**.
37. Barbey, R.; Lavanant, L.; Paripovic, D.; Schuwer, N.; Sugnaux, C.;Tugulu, S.; Klok, H. A. Polymer brushes via surface-initiated controlled radical polymerization: Synthesis, characterization, properties, and applications. Chem. Rev **2009,** *109*: 5437−5527.
38. Chen, T.; Jordana, R.; Zauscher, S. Polymer brush patterning using self-assembled microsphere monolayers as microcontact printing stamps. Soft Matter **2011**, *7,* 5532−5535.
39. Iwata, R.; Suk-In, P.; Hoven, V. P.; Takahara, A.; Akiyoshi, K.; Iwasaki, Y. Control of nanobiointerfaces generated from well-defined biomimetic polymer brushes for protein and cell manipulations. Biomacromolecules **2004**, *5,* 2308−2314.

40. Larsson, A.; Du, C. X.; Liedberg, B. UV-patterned poly(ethylene glycol) matrix for microarray applications. Biomacromolecules **2007**, *8,* 3511−3518.
41. S. Herminghaus, Wetting and dewetting in bio-related systems. J. Phys Condens. Matter **2005**, *17*, S637.
42. Liu, P.; Huang, X.; Zhou, R.; Berne, B.J. Observation of a dewetting transition in the collapse of the melittin tetramer. Nature **2005**, *437,* 159-162.
43. Valle F.; DeRose A. J.; Dietler G.; Kawe M.; Plu¨ ckthun A.; Semenza G. AFM structural study of the molecular chaperone GroEL and its two-dimensional crystals: an ideal 'living' calibration sample. Ultra microscopy **2002**, *93,* 83–89.
44. K. Appasani; R. K. Appasani, "Stem Cells and Regenerative Medicine: From Molecular Embryology to Tissue Engineering", Humana Press, **2010**.
45. Valle F.; Chelli B.;Bianchi M.;Greco P.; Bystrenova E.; Tonazzin I.; Biscarini F. Stable non-covalent large area patterning of inert Teflon-AF surface: a new approach to multiscale cell guidance. Adv. Eng. Mater, **2010**, *12,* B185–B191.
46. Ventre M.; Valle F.; Bianchi M.; Biscarini F.;Netti P. A. Cell fluidics: producing cellular streams on micro patterned synthetic surfaces. Langmuir **2011**, *28,* 714–721.
47. Buschbaum M. P. Dewetting and Pattern Formation in Thin Polymer Films as Investigated in Real and Reciprocal Space. Journal of Physics: Condensed Matter **2003**, *15*, 1549-1553.
48. Xue, L; Yanchun, H. Pattern formation by dewetting of polymer thin film Progress in Polymer Science **2011**, *11, 36*, 269–293.
49. Seeman, R; Herminghaus, S; Jacobs, K. Dewetting Patterns and Molecular Forces: A Reconcillation. Physics Review Letters **2000**, *86,* 5534-5537.
50. Rezende, C. A.; Lee, T.; Galembeck, F. Atomic Force Microscopy Applied to the Study of Dewetting Patterns of Thin Films from Polymer Solutions. Microscopy and microanalysis **2005**, 110-113.
51. "TappingMode Imaging Applications and Technology" Veeco, Inc. **2004**.
52. "Atomic Force Microscopy." Wikipedia. Wikimedia Foundation, **2014**. Web. (Accessed June 2014).
53. "TappingMode Imaging Applications and Technology" Veeco, Inc. 2004.
54. Rani M.; "Fractals: A Research." International Journal of Computer Engineering and technology. **2013**, *4*, 289-307.
55. Falconer K.; "Fractals in the real world." Fractals: A Very Short Introduction. Oxford: Oxford UP, **2013**: 102-120.

56. Witten, T. A.; Sander, L. M. Diffusion-limited Aggregation, a Kinetic Critical Phenomenon. Phys. Rev. Lett. **1981**, *47*, 1400-1403.
57. Family, F.; Masters, B. R.; Platt, D. E. Fractal Pattern Formation in Human Retinal Vessels, Physica D **1989**, *38*, 98-103.
58. Vicsek, T. Fractal Models for Diffusion Controlled Aggregation. J. Phys. A: Math. Gen. **1983**, *16,* L647-L652.
59. Polymers and Plasticizers. Argonne National Laboratory. Newton. **2011**.
60. Young R J et al., "Introduction to Polymers" 3rd ed. CRC Press. **2011**.